NANO · MICRO small
www.small-journal.com

Multifunctional Co-Delivery Systems with Downregulation of the Novel Target PIM1 in Macrophages to Ameliorate TF-Mediated Coagulopathy in Sepsis

Aiming Zhou, Jiejie Cai, Ying Wang, Rongrong Zhang, Jiang Tan, Chen Zhou, Shuang Luo, Qiuqi Gao, Yueyue Huang, Yihua Dong, Haiqing Song, and Jingye Pan**

Disordered coagulation is an independent risk factor for mortality in patients with sepsis and currently lacks effective therapeutic strategies. In this study, PIM1, a novel target predominantly expressed in macrophages during sepsis, is investigated by bioinformatics analysis and clinical evaluation in patients with sepsis compared with healthy individuals. The regulatory mechanism by which PIM1 promotes the release of tissue factors (TF) from macrophages by modulating the phosphorylation levels of mTOR through the AKT and MAPK signaling pathways is demonstrated both in vitro and in vivo. Based on these findings, a multifunctional co-delivery system based on mesoporous polydopamine (MPDA) nanoparticles (NPs) coated with cationic polyethyl eneimine (PEI) and macrophage-targeting glucomannan (GM) (MPDA@PEI@GM NPs) is proposed for the co-delivery of the PIM1 inhibitors SMI-4a and small interfering RNA (siPIM1) to downregulate PIM1 expression and improve sepsis-induced coagulopathy. MPDA@SMI-4a@PEI/siPIM1@GM demonstrates negligible cytotoxicity, excellent macrophage-targeting efficiency, prolonged blood circulation, and significantly downregulated PIM1 expression. Notably, treatment with MPDA@SMI-4a@PEI/siPIM1@GM improves the survival rates of septic mice by ameliorating disordered coagulation and alleviating lung injury. Bioinformatic analysis and clinical research-guided MPDA@SMI-4a@PEI/siPIM1@GM co-delivery systems improve TF-mediated coagulopathy in sepsis and alleviate sepsis-induced acute lung injury, marking a significant advancement in the development of clinical antisepsis therapies.

1. Introduction

Sepsis is a fatal organ dysfunction caused by an uncontrolled host response to infection and is associated with high morbidity and mortality worldwide.[1] According to two independent cohorts, sepsis accounts for one in every two to three deaths in terms of overall hospital mortality.[2] In a 2020 report in The Lancet, there were an estimated 48.9 million cases of sepsis worldwide every year and ≈11.0 million deaths from sepsis.[3] Notably, more than half of septic patients developed coagulation disorders during the disease, and 20%–50% of patients progress to disseminated intravascular coagulation (DIC). If patients with sepsis develop DIC, their mortality rate increases from 27% to 43%.[4] Consequently, disordered coagulation is an independent predictor of mortality in patients with sepsis.[4,5] However, there are limited specific recommendations for the management of sepsis-induced coagulopathy (SIC), even in the Surviving Sepsis Guidelines. Current therapeutic strategies focus on addressing the thrombotic phenotype by reintroducing exogenous anticoagulants such as activated

A. Zhou, J. Cai, J. Tan, C. Zhou, S. Luo, Q. Gao, Y. Huang, Y. Dong, J. Pan
Department of Intensive Care Unit
The First Affiliated Hospital of Wenzhou Medical University
Wenzhou, Zhejiang 32500, China
E-mail: panjingye@wzhospital.cn
A. Zhou, J. Tan, C. Zhou, S. Luo, J. Pan
Zhejiang Key Laboratory of Critical Care Medicine
Wenzhou, Zhejiang 325000, China
The ORCID identification number(s) for the author(s) of this article can be found under https://doi.org/10.1002/smll.202412688

DOI: 10.1002/smll.202412688

A. Zhou, J. Tan, C. Zhou, S. Luo, J. Pan
Wenzhou Key Laboratory of Critical Care and Artificial Intelligence
Wenzhou, Zhejiang 325000, China
A. Zhou, J. Tan, C. Zhou, S. Luo, J. Pan
Zhejiang Engineering Research Center for Hospital Emergency and Process Digitization
Wenzhou, Zhejiang 325000, China
Y. Wang, R. Zhang
Cixi Biomedical Research Institute
Wenzhou Medical University
Ningbo, Zhejiang 315302, China
H. Song
School of Engineering
Westlake University
Hangzhou, Zhejiang 310030, China
E-mail: songhaiqing@westlake.edu.cn

protein C, tissue factor pathway inhibitor, antithrombin III, and thrombomodulin.[6] However, none of these interventions has consistently demonstrated a mortality benefit in clinical studies.[7–12] Therefore, there is an urgent need to develop effective and targeted therapeutic interventions to prevent the progression of coagulopathy in sepsis.

SIC is a complex condition involving the interactions between innate immune activation and dysregulated coagulation. Extensive research has verified that tissue factor (TF) initiates the exogenous coagulation pathway and is one of the most active endogenous pro-coagulant substances. In sepsis, large quantities of TF and a large amount of cytokines are released stimulated by endotoxins and exotoxins, promoting thrombin secretion and thrombosis.[4,13,14] Furthermore, monocytes/macrophages have been identified as the primary sources of endogenous TF.[13] Myeloid cell-specific deletion of the TF gene in endotoxemic mice notably reduced plasma thrombin-antithrombin (TAT) levels.[15] In addition, knocking down the expression of endogenous TF in human blood monocytes using small interfering RNA (siRNA) resulted in a profound decline in TF activity and protein levels, whereas silencing TF in granulocytes resulted in no reduction, confirming that monocytes play a primary role in generating plasma TF in response to endotoxemia.[16] Moreover, deficiency in TF expression reduces lipopolysaccharide (LPS) -induced coagulation, inflammation, and mortality both in vivo and in vitro.[17] Our previous research demonstrated that inhibiting the expression of TF significantly decreased the plasma levels of TAT, plasminogen activator inhibitor-1 (PAI-1), and thrombin, reduced fibrin deposition and thrombosis formation and improved the survival rate of septic mice.[18–22] These results suggest that further exploration of the important endogenous factors involved in the regulation of TF production in patients with sepsis is indispensable and will provide new targets and a theoretical basis for the prevention and treatment of SIC.

PIM1 is a member of the serine/threonine protein kinase Pim family, which is highly expressed during the embryonic period in animals and gradually decreases after birth.[23] However, pathological damage causes its expression to increase again. Previous studies on PIM1 have mainly focused on its association with tumors, inflammation, and other related diseases. High PIM1 expression is closely related to poor prognosis.[24–26] Additionally, our previous study verified that the inhibition of STAT3 reduces TF expression in LPS-induced macrophages through the STAT3/NFkB/MAPK signaling pathway, normalizes disordered coagulation, and decreases mortality in septic mice.[27] Interestingly, PIM1 is a downstream effector of STAT3.[25] Drawing on these insights, we hypothesized that PIM1 may be involved in the development and progression of SIC and may regulate TF production. Thus, bioinformatics analysis and clinical studies of patients with sepsis were carried out to identify critical genes related to prognosis. These results revealed that PIM1 and PILRA were key prognosis-associated genes (PAGs), of which PIM1 was associated with a poorer outcome, whereas PILRA played the opposite role. Additionally, correlation analysis based on the Gene Expression Omnibus (GEO) datasets showed that PIM1 positively correlated with coagulation factor 2 (F2, commonly named thrombin) and factor 3 (F3, commonly named TF). Therefore, the role of PIM1 in the regulation of TF production and the underlying mechanisms were further explored in this study.

However, successful nucleic acid delivery requires safe and efficient carriers to circumvent enzymatic degradation in vivo. Non-viral vectors demonstrate lower immunogenicity, ease of modification, and higher loading capacity than viral vectors.[28,29] In this study, a multifunctional nucleic acid delivery system based on mesoporous polydopamine nanoparticles (MPDA) coated with cationic polyethyleneimine (PEI) and macrophage-targeting glucomannan (GM) nanoparticles (NPs) (MPDA@PEI@GM NPs) was developed for the co-delivery of the PIM1 inhibitor SMI-4a and siRNA interfering with PIM1 expression (siPIM1 for the treatment of sepsis (**Scheme 1**). In this study, MPDA encapsulated the hydrophobic drug SMI-4a and scavenged reactive oxygen species (ROS), whereas PEI endowed the delivery system with nucleic acid condensation abilities and prevented drug leakage. The GM coating consumed redundant positive charges, prolonged blood circulation time, and enhanced macrophage-targeting delivery efficiency. The Schiff base bonds between aldehyde GM and the amino groups of PEI break under the acidic conditions of lysosomes, increasing the positive charge of the carriers and facilitating lysosomal escape. This mechanism ensured the effective release of SMI-4a and siPIM1 into the cytoplasm. Subsequently, both the protein and mRNA expression levels of PIM1 in macrophages were significantly reduced. Furthermore, the ROS-scavenging ability of MPDA contributed to the alleviation of inflammation in sepsis. MPDA@SMI-4a@PEI/siPIM1@GM demonstrated negligible cytotoxicity, excellent targeting ability, and enhanced transfection efficiency of siPIM1. The survival rate of LPS-induced septic mice treated with MPDA@SMI-4a@PEI/siPIM1@GM increased because of the improved disordered coagulation and alleviated lung injury. Taken together, this study revealed a new therapeutic target, PIM1, and elucidated its regulatory mechanism in stimulating the release of TF from macrophages through the modulation of mTOR phosphorylation via the AKT and MAPK signaling pathways, both in vitro and in vivo. Based on this new therapeutic target, PIM1, a multifunctional nucleic acid and drug co-delivery platform, was successfully developed to ameliorate TF-mediated coagulopathy in sepsis.

2. Results and Discussion

2.1. Identification of Prognostic Genes of Sepsis through Bioinformatics Analysis and RNA-seq

We analyzed differentially expressed genes (DEGs) between patients with sepsis and healthy controls using the GSE65682 dataset from the GEO database. There were 3260 DEGs, including 1106 upregulated and 2154 downregulated genes. The volcano plot and heatmap of all DEGs in the sepsis and healthy control groups are shown in Figures S1A and S2, Supporting Information, respectively. Then Gene Ontology (GO) enrichment analysis was performed on the DEGs, which revealed significant associations with immune system processes, immune responses, and leukocyte activation (Figure S1B, Supporting Information). Therefore, we conducted an immune infiltration analysis of patients with sepsis and healthy volunteers. Using the CIBERSORT algorithm, samples from patients with sepsis generally contained a higher proportion of monocytes, M0 macrophages, and M1 macrophages than the healthy samples (Figure S1C,

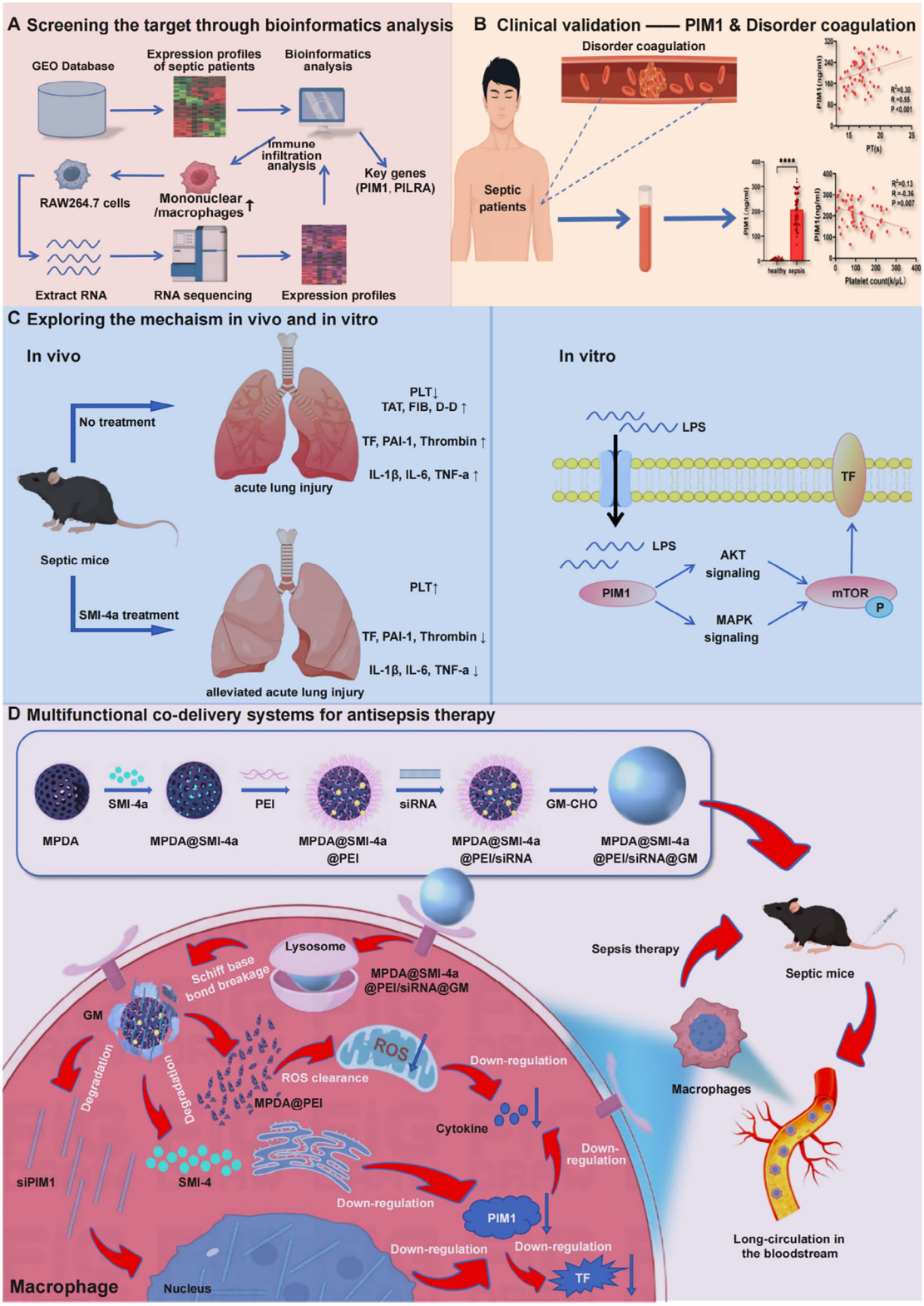

Scheme 1. Schematic illustration of A) bioinformatic analysis and B) clinical research guided novel target PIM1, C) regulatory mechanism of PIM1 for sepsis-induced coagulopathy both in vivo and in vitro, and D) the preparation of multifunctional co-delivery systems of PIM1 inhibitors and the antisepsis process in vivo.

Supporting Information). Subsequently, we focused on monocytes/macrophages, and RNA sequencing was carried out using RAW264.7, stimulated with LPS (LPS group) and without LPS (control group), and a total of 549 DEGs were screened (Figures S1D and S3, Supporting Information). The DEGs in the GSE65682 dataset intersected with DEGs in the RAW264.7 dataset, and 77 DEGs were screened (Figure S1E, Supporting Information).

To identify the PAGs, 479 patients with sepsis and survival information from the GSE65682 dataset were included. First, we conducted a Cox regression analysis on the 77 DEGs and 12 PAGs (CLEC4E, PILRA, PIM1, CCL4, NFKBIZ, SOCS2, IL1R2, TBC1D4, IFIT2, EHD1, PDE4B, and CBFA2T3) were selected among the statistically significant variables to build a prognosis-related risk score (PRRS) model (Model 1) (**Figure** 1A), which demonstrated a good judgment efficacy (area under the curve [AUC] = 0.8, p <0.05) (Figure S1F, Supporting Information). Moreover, the 28-day survival rate significantly declined in patients with high-risk scores in Model 1 (hazard rate [HR] = 6.8, p <0.05) (Figure S1G, Supporting Information).

Subsequently, LASSO-Cox regression analysis, which defined variables by seeking the value that corresponded to the lowest possible likelihood of classification error[30,31] was utilized to screen the optimal PAGs from the 77 DEGs screened above. After incorporating the variables into the LASSO-Cox regression model with minimized lambda, 6 DEGs (PIM1, PTX3, CCL5, ARHGEF3, PILRA, and TBCID4) were selected to build the PRRS model (Model 2) (Figure S4A,B, Supporting Information). The association between the expression levels of the six DEGs and survival is also illustrated in a forest plot (Figure 1B). The expression levels of PIM1 and PTX3 were found to have significantly positive contributions to poor prognosis, whereas the expression levels of CCL5 and PILRA had opposite effects (Figure 1B). When evaluating the prognostic efficacy of Model 2 based on the AUC, we found that Model 2 was a moderate indicator of sepsis prognosis (AUC = 0.7, $p < 0.05$). The higher risk score in Model 2 was associated with a higher 28-day mortality rate in patients with sepsis (Figure S4C,D, Supporting Information).

Based on these two PRRS models, PIM1 and PILRA were identified as overlapping genes (Figure 1C). Gene expression levels of these two key PAGs were investigated using the GSE65682 dataset. The results showed that the expression of PIM1 was upregulated in patients with sepsis, whereas that of PILRA was downregulated (Figure 1D). Based on the 28-day survival data, we found that the expression level of PIM1 was higher in the non-survivor group than in the survivor group. However, a high PILRA expression was associated with better outcomes (Figure 1E). Furthermore, Kaplan-Meier survival analysis indicated that the PIM1 high-expression group exhibited a poorer 28-day survival rate than the low-expression group (Figure 1F), whereas higher expression of PILRA contributed to a better prognosis (Figure S5A, Supporting Information). Receiver-operating characteristic curves were used to evaluate the ability of PIM1 and PILRA to predict sepsis, and the receiver-operating characteristic (ROC) curves were employed. The AUC of PIM and PILRA were greater than 0.70, and the predictive value of PIM1 was higher than that of PILRA (Figures 1G and S5B, Supporting Information). To further explore the expression features of PIM1, we observed that PIM1 was mainly expressed by macrophages in the lung tissue, according to the Human Protein Atlas (Figure S5C, Supporting Information). Taken together, bioinformatics analysis revealed that PIM1 and PILRA are key PAGs in sepsis. PIM1 was associated with a poor prognosis, which is consistent with previous studies,[24–26] whereas PILRA contributed to a better outcome, and both were good predictors of sepsis. In this study, PIM1 markers identified through bioinformatics analysis were focused on exploring their role in patients with sepsis because it is a downstream target of STAT3[25] which has been confirmed to play a significant role in sepsis-associated coagulation in our previous work.[27]

2.2. Correlation Analysis of PIM1 and Sepsis-Associated Coagulation based on Clinical Research

First, correlation analysis was performed to further investigate the relationship between PIM1 and coagulation factors F2 and F3. **Figure** 2A,B shows the correlation coefficient of R = 0.54 (p = 1.5e–37) between PIM1 and coagulation F2, and a correlation coefficient of R = 0.62 (p = 2.3e–52) between PIM1 and F3. These results indicate a remarkable positive correlation between PIM1 and the coagulation factors F2 and F3. Simultaneously, the PIM1 levels in patients with sepsis, healthy controls, patients with DIC, patients without DIC, patients with SIC, and patients without SIC were evaluated. As shown in Figure 2C, PIM1 was highly increased in the plasma of patients with sepsis compared to that in healthy controls ($p < 0.001$), which is in line with the results of RNA sequencing from the GSE65682 dataset (Figure 1D). Notably, PIM1 levels in patients with DIC were significantly higher than those in patients without DIC (p = 0.002) (Figure 2D). In addition, the level of PIM1 in patients with SIC was higher than that in patients without SIC (p = 0.037) (Figure 2E). These results indicate that increased PIM1 levels are potential diagnostic criteria for sepsis and are promising for predicting DIC and SIC. Furthermore, the diagnostic accuracy of the PIM1 level was assessed via ROC analysis (Figure 2F). AUC ranging from 0.5 to 1.0 is a measure of the overall diagnostic accuracy of the test, and the cutoff value calculated from the curve provided the highest sensitivity and specificity.[32] From the ROC curve (Figure 2F), the cutoff value of PIM1 was 41.99 ng mL^{-1} for sepsis diagnosis (AUC = 1.00, $p < 0.05$), indicating the excellent diagnostic assurance of plasma PIM1 for sepsis. In addition, a cutoff value of 270.7 ng mL^{-1} of PIM1 for DIC diagnosis (AUC = 0.77, p <0.05) and 181.3 ng mL^{-1} for SIC diagnosis (AUC = 0.70, p <0.05), respectively, were observed. These results revealed a significant diagnostic assurance of PIM1 for DIC and SIC diagnoses.

Based on these results, the relationship between PIM1 and coagulation in a clinical setting was further explored. PIM1 was positively correlated with parameters typically elevated in DIC[33] including prothrombin time (PT) (R = 0.55, Figure 2G), international normalized ratio (INR) (R = 0.54, Figure 2H), and activated partial thromboplastin time (APTT) (R = 0.51, Figure 2I). Conversely, PIM1 expression was inversely correlated with platelet count, which is known to decline in patients with DIC (R = 0.36, Figure 2J). In addition, the relationship between PIM1 expression and mortality in patients with sepsis was explored. PIM1

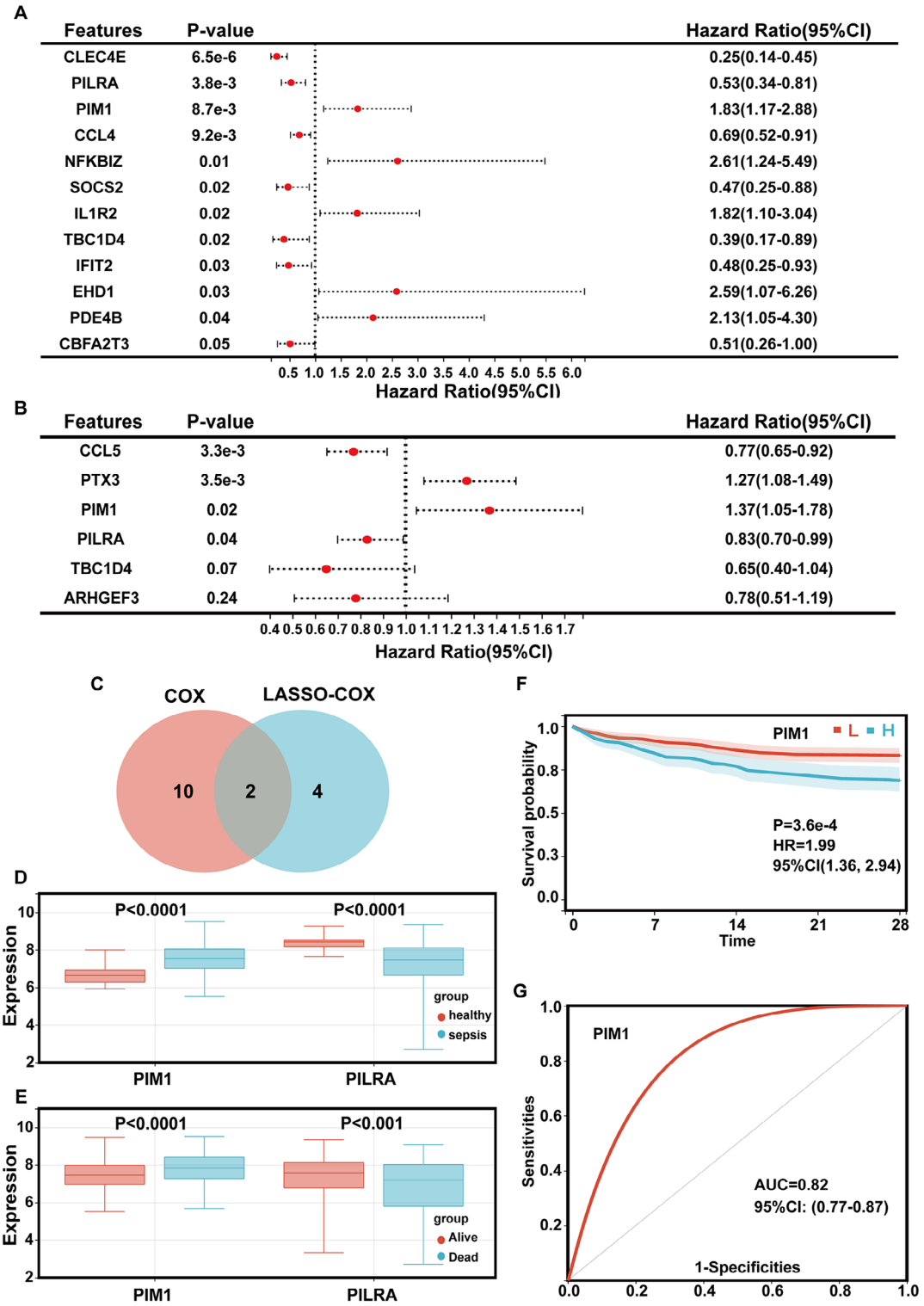

Figure 1. Identification and screening of key prognosis-related genes. A) Forest plots illustrate the findings of a multivariate Cox regression analysis examining the relationship between the PRGs and 28-day survival in patients with sepsis. B) Forest plot of the associations between the six prognostic molecules and 28-day survival in patients with sepsis. C) Venn diagram of PRGs from Cox regression analysis and LASSO-Cox regression analysis. D) Expression of two key PRGs (PIM1 and PILRA) in patients with sepsis and healthy controls. E) Expression of PIM1 and PILRA in dead group and alive group among patients with sepsis. F) Kaplan-Meier curve of 28-day survival for patients with sepsis and high and low expression of PIM1. G) ROC curves of PIM1 for the prediction of sepsis. Each bar represents the mean ± SD. The comparison between the two groups was performed using unpaired Student t-tests (D and E).

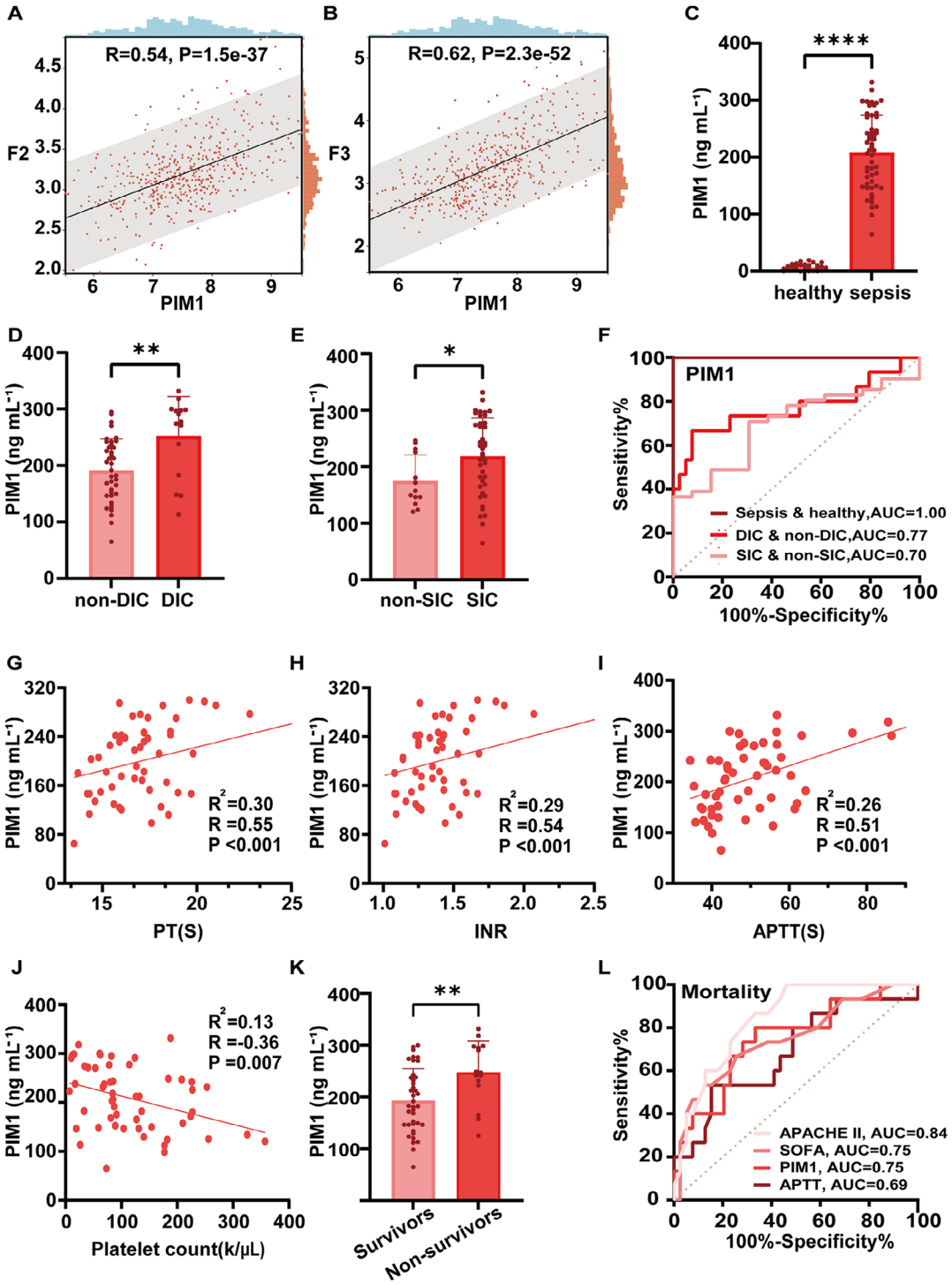

Figure 2. Elevated expression of PIM1 correlates with disordered coagulation in patients with sepsis. A,B) Scatter plot and linear regression analysis between PIM1 and coagulation factors (F2 and F3) in the GSE65682 dataset. C) Plasma PIM1 levels by ELISA between healthy control and patients with sepsis. D) Plasma PIM1 levels by ELISA between patients with sepsis with and without DIC. E) Plasma PIM1 levels by ELISA between patients with sepsis with and without SIC. F) ROC curve for plasma PIM1 to discriminate between patients with sepsis and healthy volunteers, patients with DIC and non-DIC sepsis, and patients with SIC and non-SIC sepsis. G–J) Scatter plot and linear regression analysis between ELISA PIM1 and laboratory measurements of (G) PT, (H) INR, (I) APTT, and (J) platelet count. K) Plasma PIM1 levels by ELISA in patients with sepsis between survivors and non-survivors. L) ROC curves for PIM1, APTT, SOFA score, and APACHEII score to predict 28-day mortality in patients with sepsis. ELISA, enzyme-linked immunosorbent assay; DIC, disseminated intravascular coagulation; SIC, sepsis-induced coagulation; SOFA, sequential organ failure assessment; APACHE, acute physiology and chronic health evaluation. Each bar represents the mean ± SD. The comparison between the two groups was performed using an unpaired Student's *t*-test (C-E and K). * $p < 0.05$, ** $p < 0.01$, **** $p < 0.0001$.

Table 1. Clinical parameters based on plasma PIM1 levels. Plasma PIM1 levels at admission were dichotomized by an optimal cutoff of 270.7 ng mL^{-1} defined by ROC analysis for plasma PIM1 in differentiating patients with DIC risk factors. Levels of fibrinogen within each classification are displayed as mean ± standard deviation, whereas the levels of other clinical parameters are displayed as median (interquartile range). SOFA, sequential organ failure assessment; APACHE, acute physiology, and chronic health evaluation.

Basic information	PIM1 > 270.7 ng mL^{-1} (n = 13)	PIM1 ≤ 270.7 ng mL^{-1} (n = 41)	*p*-value
APTT (s), median (IQR)	56.80 (49.60–80.90)	44.1 (40.05–53.55)	<0.001
PT (s), median (IQR)	20.40 (17.20–28.60)	16.70 (15.30–17.80)	<0.001
INR, median (IQR)	1.80 (1.45–2.76)	1.35 (1.23–1.44)	<0.001
Fibrinogen(g L^{-1}), median (IQR)	4.09 ± 2.07	4.98 ± 1.51	0.020
Platelet count(k μL^{-1}), median (IQR)	61.00 (17.50–98.00)	127.00 (76.50–196.00)	0.003
Lactate(mg dL^{-1}), median (IQR)	7.80 (5.90–11.20)	3.20 (2.23–4.70)	<0.001
SOFA Score, median (IQR)	14.00 (6.00–16.00)	5.00 (3.00–8.00)	0.002
APACHEII Score, median (IQR)	24.00 (15.50–32.50)	13.00 (9.5–18.00)	0.002

expression was much higher in the non-survivor group than in the survivor group (p = 0.005, Figure 2K), which implied that PIM1 levels might be used as a death warning. The performance of PIM1, coagulation indices, and disease severity scores in predicting the mortality of patients with sepsis was assessed using ROC curves. As shown in **Table 1**, patients in the high PIM1 group (> 270.7 ng mL^{-1}) demonstrated significantly prolonged APTT, PT, and INR (all $p < 0.001$) and decreased platelet counts (p = 0.003) and fibrinogen levels (p = 0.020) compared with those in the low PIM1 group (< 270.7 ng mL^{-1}). Notably, disease severity scores, including the SOFA (p = 0.002) and APACHE II scores (p = 0.002), were higher in the high PIM1 group than in the low PIM1 group. To further investigate the ability of PIM1 to predict mortality, the ROC curve of PIM1 compared to the APACHE II score, SOFA score, and APTT for mortality was plotted. The results showed that PIM1 had a similar ability to predict mortality as the SOFA score and more accurately predicted mortality (AUC = 0.75) than the traditional coagulation indices, including PT (AUC = 0.66), APTT (AUC = 0.69), INR (AUC = 0.67), and platelet count (AUC = 0.53) (Table S1, Supporting Information, Figure 2L). These results demonstrated that high PIM1 was not only linked to traditional coagulation parameters but also an accurate predictor of patient outcomes. High PIM1 expression correlated with sepsis-induced acute lung injury (SI-ALI) and coagulation activation in septic mice was demonstrated in an LPS-induced septic mouse model (Figure S6, Supporting Information), which is consistent with the above clinical research results (Figure 2).

2.3. PIM1 Inhibition Protects Septic Mice from Coagulation Activation and SI-ALI

To assess whether PIM1 mediates coagulation cascades during sepsis, mice were administered SMI-4a or vehicle. This procedure is depicted as a timeline in **Figure 3**A. We confirmed the suppression of PIM1 expression in SMI-4a-treated mice using western blotting and RT-qPCR (Figure 3B–D). We observed that SMI-4a treatment resulted in a notable increase in platelet count, along with a significant reduction in plasma TAT, D-dimer, and fibrinogen (Figure 3E–H). In the lung tissue, we observed reduced fibrin deposition (Figure 3I) and decreased TF, PAI-1, and thrombin expression after treatment with SMI-4a (Figure 3–N), indicating that sepsis-induced coagulation activation was attenuated. In addition, the histopathological analysis of septic mouse lung sections showed alleviated alveolar edema with reduced microthrombus formation and alveolar thickness after treatment with SMI-4a (Figure 3I). Consistently, macrophage infiltration in the lungs was ameliorated, with reduced inflammatory cytokine production in the SMI-4a-treated group (Figure 3I, O–Q). Furthermore, we measured the survival rates of septic mice treated with and without SMI-4a and found that the PIM1 inhibitor, SMI-4a, markedly improved the survival rate of septic mice (Figure 3R). These findings support the important role of PIM1 in mediating the activation of coagulation and SI-ALI.

2.4. PIM1 Inhibition Reduces the Expression of TF in Macrophages by Downregulating mTOR Phosphorylation

Clinically, patients with sepsis commonly have abnormal exogenous coagulation pathways, pathogens, microbial toxins, and endogenous danger signals that induce macrophages and endothelial cells to release TF in large amounts, thus activating exogenous coagulation pathways and secreting thrombin.[34] According to our results, PIM1 positively correlated with TF at the transcriptome level as well as with PT, a common screening test used to detect the function of the exogenous coagulation system. PIM1 is widely expressed in macrophages and is a common source of TF.[33] Therefore, we hypothesized that high expression of PIM1 in sepsis contributes to the abnormal expression of TF in macrophages.

To test this hypothesis, we conducted in vitro experiments using RAW264.7 cells. First, we assessed the cytotoxic effects of SMI-4a on RAW264.7, using CCK8 assays. The results indicated that SMI-4a concentration ranging from 0–80 μM was non-toxic (Figure S7A, Supporting Information), and 80 μM was identified as the optimal concentration for use in RAW264.7 cells (Figure S7B–F, Supporting Information). Then, we treated RAW264.7 cells with or without SMI-4a (80 μM) for 1 h before being stimulated with LPS (1 μg mL^{-1}) for 6 h in subsequent experiments. Subsequently, we measured the levels of PIM1 and TF in macrophages by western blotting and IF staining. These two indicators were enhanced by LPS stimulation and weakened

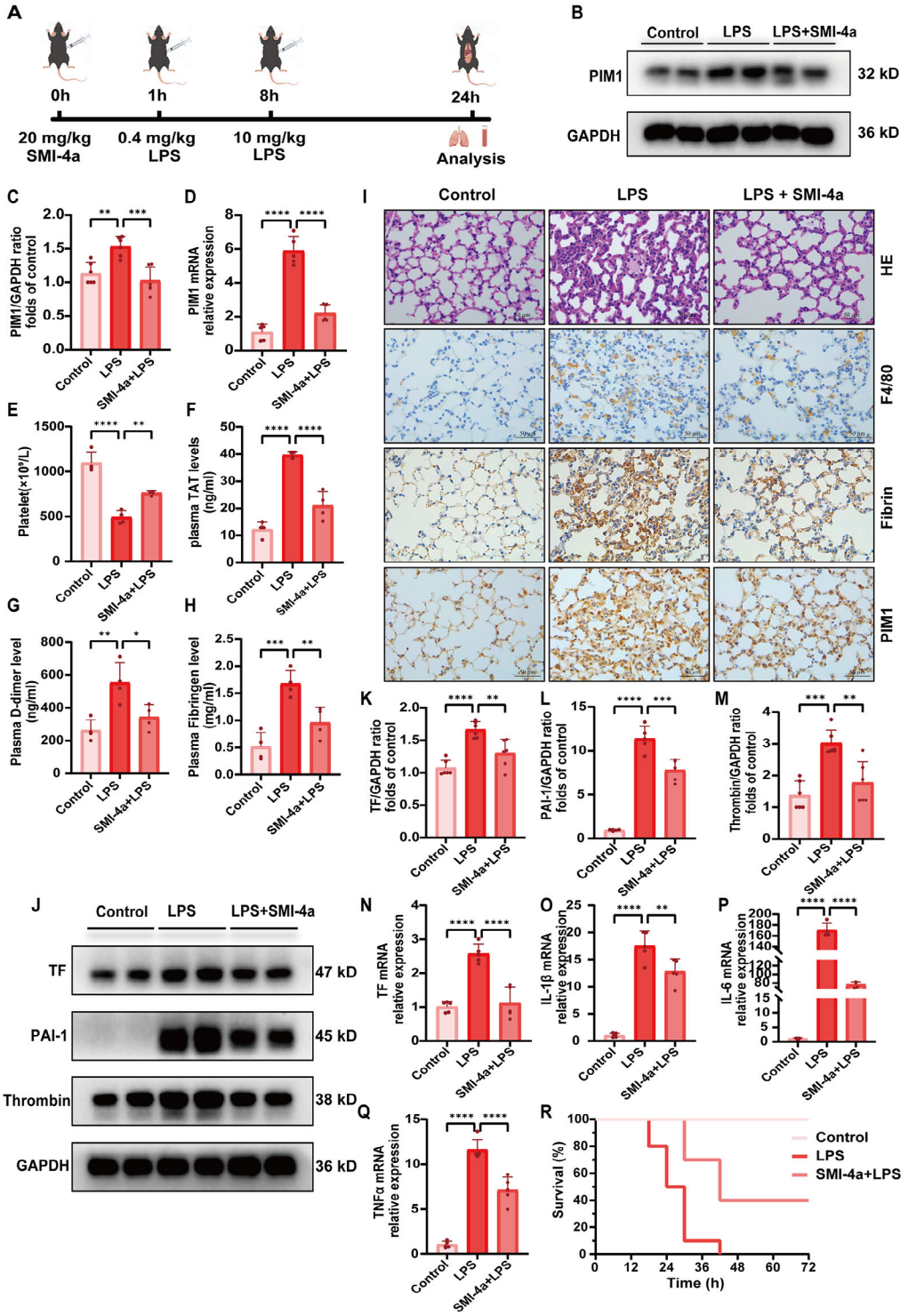

Figure 3. PIM1 inhibitor SMI-4a protects septic mice against coagulation activation and sepsis-induced acute lung injury. A) Schematic representation of animal experimental procedures. B) Representative western blot membranes and corresponding densitometric analyses of (C) PIM1 in lung tissue (n = 6/group). D) mRNA levels of PIM1 in murine lung tissues (n = 5/group). E) Platelet count in mice (n = 4/group). F–H) Plasma levels of coagulation-related factors in mice plasma by ELISA, including (F) TAT, (G) D-dimer, and (H) fibrinogen (n = 4/group). I) The lung sections were subjected to hematoxylin and eosin (HE) staining, F4/80, fibrin, and PIM1 immunohistochemical analysis (n = 4/group; scale bar:50 μm). J) Representative western blot membranes and corresponding densitometric analyses of (K) TF, (L) PAI-1, (M) Thrombin in lung tissue (n = 6/group). N) mRNA levels of TF in murine lung tissues (n = 5/group). O–Q) mRNA levels of (O) IL-1β, (P) IL-6, and (Q) TNF-α in murine lung tissues (n = 5/group). R) Survival curves of mice in all groups (n = 10/group). Each bar represents the mean ± SD. Statistical analysis for three or more groups was carried out using one-way ANOVA (C-H and K-Q). * $p < 0.05$, ** $p < 0.01$, *** $p < 0.001$, **** $p < 0.0001$.

by the treatment of SMI-4a (**Figures** 4A–D and S7G, Supporting Information). RT-qPCR analysis showed that both TF and PAI-1 were increased by LPS stimulation and decreased by SMI-4a treatment (Figure 4E,F), along with the inflammatory factors including IL-1β, IL-6, and TNF-α (Figure 4G–I). These findings are consistent with our hypotheses.

To further reveal the downstream pathway of PIM1, we carried out the RNA transcriptome sequencing analysis using RAW264.7 cells (control group, A) and LPS-induced RAW264.7 cells without (LPS group, B) or with SMI-4a treatment (SMI-4a+LPS group, C). We first identified the DEGs between the LPS group (B) and the control group (A), named the BVSA dataset (Figures S1D and S3, Supporting Information). The CVSB dataset included DEGs identified between the SMI-4a+LPS (C) and LPS (B) groups (Figure S7H,I). We performed KEGG pathway cluster analysis for DEGs between the LPS and SMI-4a + LPS groups (Figure 4J). The bubble chart shows that complement and coagulation cascades were enriched. We then collected coagulation pathways from the KEGG database (https://www.genome.jp/kegg/), including hsa04610 and hsa04611. A total of 203 genes in these two pathways served as coagulation-related genes (CRGs). Twenty-two DEGs were found to overlap between the BVSA dataset and CRGs, named the BVSA|Coagulation dataset, whereas 21 DEGs were observed between the CVSB dataset and CRGs, named the CVSB|Coagulation dataset (Figure S8A,B, Supporting Information). In total, five key genes, TF, PAI-2, CFB, F10, and PROCR, were discovered by overlapping DEGs from BVSA|Coagulation and CVSB|Coagulation datasets (Figure S8C, Supporting Information). The expression of key genes was measured using RT-qPCR, and the results showed that the expression of these genes was consistent with the trend observed in the microarray analysis (Figure S8D–G, Supporting Information), indicating that the RNA-seq data were reliable.

In addition, the AKT and MAPK pathways were enriched downstream of PIM1 from the bubble chart (Figure 4J). Because mTOR is a common downstream signaling molecule of both AKT and MAPK signaling pathways,[35] we assumed that the ameliorative effect of the PIM1 inhibitor SMI-4a was achieved by downregulating mTOR phosphorylation levels via the AKT and MAPK signaling pathways, thus reducing the release of TF (Figure 4K). We detected changes in these signaling pathways in vivo. The levels of p-AKT, p-ERK, p-mTOR, and p-p70s6k were notably increased in the LPS group and significantly decreased in the SMI-4a+LPS group (Figure 4L–P). Consistently, the levels of p-AKT, p-ERK, p-mTOR, and p-p70s6k were increased by LPS stimulation and decreased by SMI-4a treatment in vitro (Figures 4Q and S8H–K, Supporting Information). To further evaluate whether mTOR mediated the effect of PIM1 on the release of TF in macrophages, we blocked the activity of mTOR in LPS-induced RAW264.7 cells by using rapamycin (a specific mTOR inhibitor). Compared with the LPS group, the inhibitor group showed a notable reduction in TF mRNA and protein expression (Figure S8L–N, Supporting Information). The levels of p-mTOR and p-p70s6k were significantly decreased in the inhibitor group after LPS stimulation (Figure S8O–Q, Supporting Information). Together, these data suggested that the PIM1 inhibitor SMI-4a reduced the expression of TF in macrophages by downregulating the phosphorylation of mTOR.

2.5. PIM1 Deficiency Reduces TF Expression in Macrophages by Attenuating mTOR Phosphorylation

To further confirm the intracellular signaling components that mediate the modulatory effect of PIM1-induced TF expression, we first knocked down PIM1 expression in RAW264.7 cells using siRNA and then stimulated the cells with LPS. Both RT-qPCR and western blot analyses verified that PIM1 was effectively knocked down (**Figure** 5A–C) in macrophages. PIM1 knockdown significantly decreased the expression of PIM1, TF, and PAI-1 (Figure 5D–I), along with the expression of proinflammatory (IL-1β, IL-6, and TNF-α) in the cells stimulated by LPS (Figure 5J–L). Subsequently, we measured the expression of p-AKT, p-ERK, p-mTOR, and p-p70s6k by western blotting, and the results showed that PIM1 knockdown significantly reduced all these signaling molecules in LPS-treated macrophages (Figure 5M–R). These results suggest that PIM1 knockdown decreases TF expression by inhibiting mTOR phosphorylation and AKT and MAPK signaling pathways.

2.6. Synthesis and Characterization of MPDA@SMI-4a@PEI NPs

As shown in **Figure** 6A, SMI-4a was loaded onto MPDA to produce MPDA@SMI-4a, and PEI was coated to obtain MPDA@SMI-4a@PEI NPs. The particle size and dynamic light scattering (DLS) results revealed that the hydration radius of MPDA NPs was ≈182.1 nm, whereas the hydration radius of MPDA@SMI-4a@PEI NPs was increased to 214.9 nm (Figure 6B). The surface charge of MPDA@SMI-4a@PEI NPs increased from $^{-}$24.2 to 35.3 mV (Figure 6C), which implied that the PEI coating was successful. In addition, transmission electron microscopy (TEM) images demonstrated that MPDA had numerous mesoporous surface structures and cavities, which provided sufficient space for SMI-4a loading. After the PEI coating, the pores on the MPDA surface were covered, which was beneficial for preventing drug leakage (Figure 6D). Subsequently, the ability to scavenge intracellular ROS of MPDA@SMI-4a@PEI was assessed by flow cytometry using a ROS assay kit. The level of ROS increased in cells stimulated by LPS, but decreased after treatment with MPDA@SMI-4a@PEI (Figure 6E,F), showing the good ability to scavenge intracellular ROS of MPDA@SMI-4a@PEI.

2.7. In Vitro Antisepsis Ability of MPDA@SMI-4a@PEI/siPIM1@GM

High transfection efficiency and low toxicity should be balanced for a successful delivery system. The cytotoxicity and transfection ability of MPDA@SMI-4a@PEI/siPIM1@GM at various mass ratios were assessed in RAW264.7 cells. As shown in Figure 6G, MPDA@SMI-4a@PEI NPs exhibited negligible cytotoxicity in RAW264.7 cells even at the mass ratio of 40:1. In contrast, the in vitro transfection results for MPDA@SMI-4a@PEI/siPIM1 showed that the mRNA expression of PIM1 was the lowest at a mass ratio of 30:1 (Figure S9A, Supporting Information). Based on the optimum mass ratio of 30:1 for MPDA@SMI-4a@PEI to siPIM1, the transfection efficiency of MPDA@SMI-4a@PEI/siPIM1@GM was evaluated

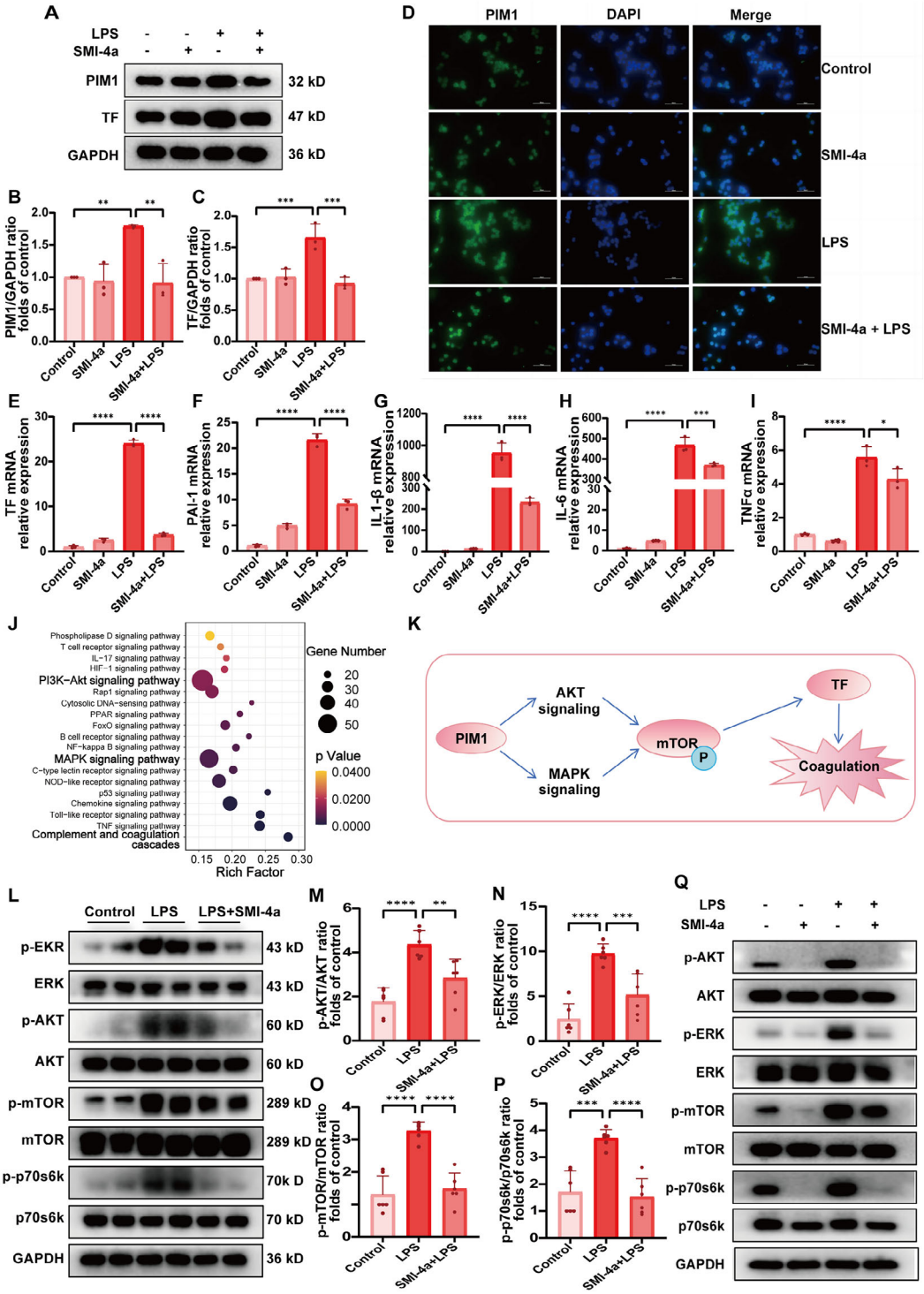

Figure 4. PIM1 inhibitor SMI-4a reduces TF expression by downregulating mTOR phosphorylation via the AKT and MAPK pathways in vivo and in vitro. A) Representative western blot membranes and corresponding densitometric analyses of (B) PIM1 and (C) TF in RAW264.7 cells (n = 3/group). D) Representative images of immunofluorescence staining of PIM1 in RAW264.7 cells (400 ×, scale bar: 50 μm). E–I) mRNA levels of (E) TF, (F) PAI-1, (G) IL-1β, (H) IL-6, and (I) TNF-α in RAW264.7 cells (n = 3/group). J) KEGG enrichment analysis of DEGs between RAW264.7 cells with and without SMI-4a pretreated before stimulation of LPS. K) Schematic diagram of the potential signaling pathways involved between PIM1 and coagulation activation in sepsis. L) Representative western blot membranes and corresponding densitometric analyses of (M) p-AKT, (N) p-ERK, (O) p-mTOR, and (P) p-p70s6k in lung tissue (n = 6/group). Q) Representative western blot membranes of p-AKT, p-ERK, p-mTOR, and p-p70s6k in RAW264.7 cells (n = 3/group). Each bar represents the mean ± SD. Statistical analysis for three or more groups was carried out using one-way ANOVA (B-C, E-I, and M-P). * $p < 0.05$, ** $p < 0.01$, *** $p < 0.001$, **** $p < 0.0001$.

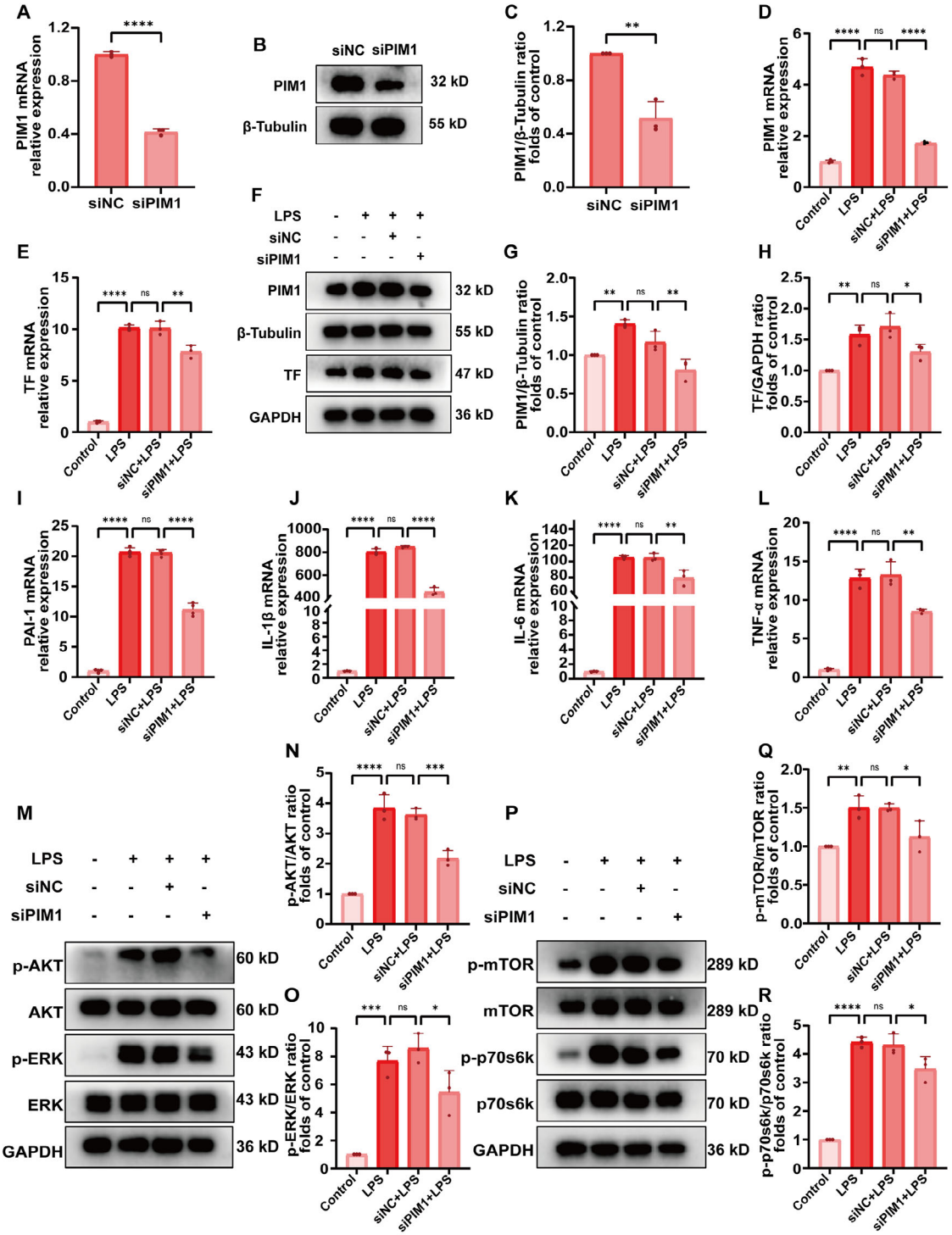

Figure 5. PIM1 knockdown reduces the expression of TF in RAW264.7 cells stimulated with LPS by downregulating mTOR phosphorylation via the AKT and MAPK pathways. A) mRNA expression of PIM1 in RAW264.7 cells transfected with siNC or siPIM1. B) Western blot images and corresponding densitometric analyses of (C) PIM1 expression in RAW264.7 transfected with siNC or siPIM1. D, E) mRNA expression of (D) PIM1 and (E) TF in RAW264.7 cells transfected with siNC or siPIM1 under stimulation of LPS. F) Western blot images and corresponding densitometric analyses of (G) PIM1 and (H) TF in RAW264.7 cells transfected with siNC or siPIM1 under stimulation of LPS. I–L) mRNA expression of (I) PAI-1, (J) IL-1β, (K) IL-6, and (L) TNF-α in RAW264.7 cells transfected with siNC or siPIM1 under stimulation of LPS. M, P) Western blot images and corresponding densitometric analyses of N) p-AKT, O) p-ERK, Q) p-mTOR, and R) p-p70s6k in RAW264.7 cells transfected with siNC or siPIM1 under stimulation of LPS. Each bar represents the mean ± SD. Statistical analysis for three or more groups was carried out using one-way ANOVA (A, C–E, G–L, N,O, and Q,R). * $p < 0.05$, ** $p < 0.01$, *** $p < 0.001$, **** $p < 0.0001$.

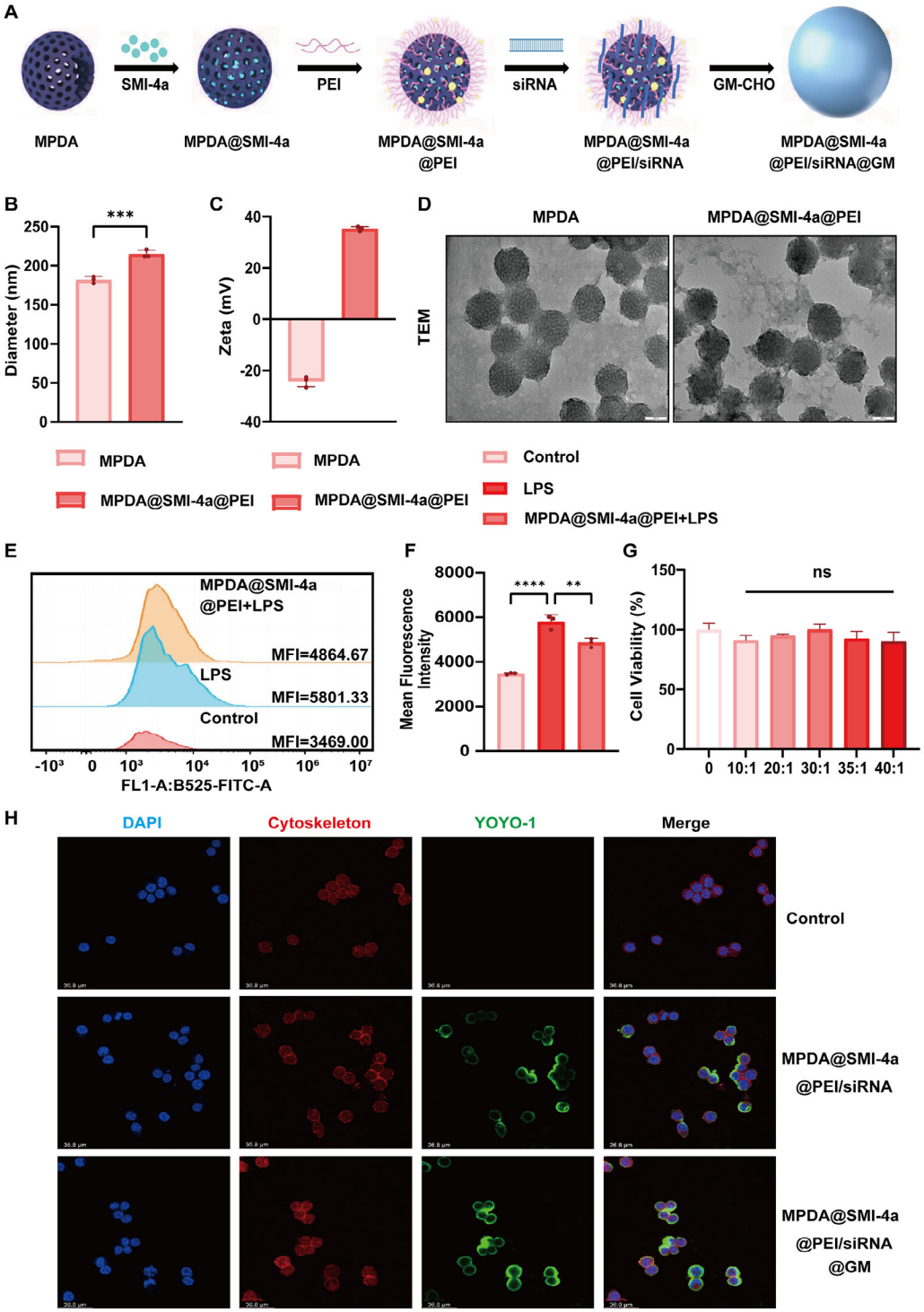

Figure 6. Preparation and characterization of NPs. A) Schematic diagram of the design and synthesis of MPDA@SMI-4a@PEI NPs. B,C) DLS measurements of hydrodynamic size (diameter) and zeta potential of NPs. D) Morphology assessment of MPDA and MPDA@SMI-4a@PEI using TEM). E,F) Flow cytometry detection of ROS levels in RAW264.7 cells pretreated with or without MPDA@SMI-4a@PEI before stimulated with LPS (n = 3). G) Cell viability (CCK-8) of RAW264.7 cells was incubated with different mass ratios of MPDA@SMI-4a@PEI NPs for 24h. H) Confocal fluorescence microscopy images to monitor the uptake of NPs by RAW264.7 cells. The cytoskeleton was stained with phalloidin (red), green fluorescence was added during material preparation, and nuclei were stained with DAPI (blue). Scale bars: 36.8 μm. Each bar represents the mean ± SD. The comparison between the two groups was performed using an unpaired Student's *t*-test (B). Statistical analysis for three or more groups was carried out using one-way ANOVA (F and G). * $p < 0.05$, ** $p < 0.01$, *** $p < 0.001$, **** $p < 0.0001$.

using various mass ratios of siPIM1 and GM. As shown in Figure S9B, Supporting Information, the mRNA level of PIM1 in MPDA@SMI-4a@PEI/siPIM1@GM-treated RAW264.7 cells slightly decreased with the increase of GM. The relative value of PIM1 mRNA was 0.76 at a mass ratio of 30:1, whereas that was 1.0 at a mass ratio of 0, indicating the targeting ability of GM RAW264.7. Surprisingly, the mRNA level of PIM1 in MPDA@SMI-4a@PEI/siPIM1@GM-treated RAW264.7 cells which pretreated with LPS decreased with the increase of GM. The relative values of PIM1 mRNA were 1.00, 0.71, 0.71, and 0.47 at mass ratios of 0, 10:1, 20:1, and 30:1, respectively (Figure S9C, Supporting Information). This excellent transfection efficiency was attributed to the ability of GM to target intracellular endocytosis. In addition, the relative value of PIM1 mRNA in RAW264.7 with LPS pretreated was lower than that without LPS pretreated, which implies the outstanding targeting ability of MPDA@SMI-4a@PEI/siPIM1@GM to RAW264.7 in sepsis.

Flow cytometry was used to verify the cellular uptake efficiency of MPDA@SMI-4a@PEI/siPIM1@GM mediated RAW264.7 presented strong fluorescence intensity compared to MPDA@SMI-4a@PEI/siPIM1 (Figure S9D,E, Supporting Information), demonstrating the targeting ability of GM, which was in agreement with the transfection efficiency. The cellular uptake of MPDA@SMI-4a@PEI/siPIM1@GM compared with that of MPDA@SMI-4a@PEI/siPIM1 and the control was visualized using a confocal microscope, where siPIM1 was labeled with YOYO-1 (green fluorescence), the cytoskeleton was stained with phalloidin (red), and the nuclei were stained with DAPI (blue). MPDA@SMI-4a@PEI/siRNA@GM-treated RAW264.7 cells showed stronger green fluorescence signals than the MPDA@SMI-4a@PEI/siRNA-treated and control groups (Figure 6H). This result indicated the excellent targeting ability of the MPDA@SMI-4a@PEI/siPIM1@GM delivery system, which resulted in enhanced transfection efficiency (Figure S9A,B, Supporting Information). Taken together, these results indicate that the MPDA@SMI-4a@PEI/siPIM1@GM delivery system possesses good targeting ability and might be a promising strategy for sepsis therapy in vivo.

To evaluate the knockdown effect, we measured the expression of PIM1 in RAW264.7 cells treated with different NPs by western blotting. The expression of PIM1 in the MPDA@SMI-4a@PEI/siPIM1@GM group was the lowest among the three groups, followed by that in the MPDA@SMI-4a@PEI/siPIM1 group (**Figure** 7A–B). In LPS-induced macrophages, the expression of PIM1 and TF was significantly reduced after treatment with MPDA@SMI-4a@PEI/siPIM1 and MPDA@SMI-4a@PEI/siPIM1@GM compared to the LPS group, and the MPDA@SMI-4a@PEI/siPIM1@GM group had lower PIM1 and TF expression than the MPDA@SMI-4a@PEI/siPIM1 group (Figure 7C–G). These results indicate that MPDA@SMI-4a@PEI NPs can successfully deliver siPIM1 to RAW264.7 cells, effectively knocking down PIM1 and decreasing TF mRNA and protein levels, and aldehyde GM modification enhanced the above effects. In addition, we found that the inflammatory factors IL-1β, IL-6, and TNF-α decreased after treatment with NPs in comparison with the LPS group. The aldehyde GM-modified NP-treated group was lower than the NP-treated group (Figure 7I–K), which indicated that MPDA@SMI-4a@PEI/siPIM1 inhibited the expression of inflammatory factors in macrophages and was enhanced after aldehyde GM modification.

2.8. In Vivo Antisepsis Ability of MPDA@SMI-4a@PEI/siPIM1@GM

To explore in vivo biodistribution, MPDA@SMI-4a@PEI/siPIM1 and MPDA@SMI-4a@PEI/siPIM1@GM, where MPDA@SMI-4a@PEI was labeled with Cy5.5, were injected with LPS, and the distribution of NPs in major organs was observed using an in vitro imaging system 4 h, 8 h, and 16 h after administration. As shown in **Figure** 8A, the accumulation of MPDA@SMI-4a@PEI/siPIM1@GM in the lung, kidney, and liver of sepsis model mice was higher than that of normal control mice at all time points, and the highest accumulation was at 16 h among the three time points (4, 8, and 16 h). Moreover, the accumulation of MPDA@SMI-4a@PEI/siPIM1@GM in the lungs, kidneys, and livers of the sepsis model mice was higher than that of MPDA@SMI-4a@PEI/siPIM1at 4 h, along with that 8 h and 16 h. These results indicate that GM assisted MPDA@SMI-4a@PEI/ siPIM1@GM in rapidly targeting and accumulating in lungs with high macrophage infiltration to knock down the expression of PIM1 in macrophages and further normalize disordered coagulation and lung injury.

To evaluate the therapeutic effects, we first measured the survival rates of sepsis mice treated with different NPs. The survival curves showed that LPS-induced septic mice all died within 42 h, whereas the survival rate treated with MPDA@SMI-4a@PEI/siPIM1 and MPDA@SMI-4a@PEI/siPIM1@GM group was 40% and 75%, respectively (Figure 8B). These results indicate the efficient antiseptic activity of MPDA@SMI-4a@PEI/siPIM1@GM. As shown in Figure 8C,D, western blotting revealed that the expression of PIM1 in MPDA@SMI-4a@PEI/siPIM1- and MPDA@SMI-4a@PEI/siPIM1@GM-treated septic mice was significantly decreased. The MPDA@SMI-4a@PEI/siPIM1@GM group demonstrated lower PIM1 expression than the MPDA@SMI-4a@PEI/siPIM1 group. Moreover, PIM1 mRNA levels decreased in both the MPDA@SMI-4a@PEI/siPIM1 and MPDA@SMI-4a@PEI/siPIM1@GM groups, whereas those in the MPDA@SMI-4a@PEI/siPIM1@GM group were much lower (Figure 8E). These results implied that the enhanced transfection ability of MPDA@SMI-4a@PEI/siPIM1@GM resulted from the macrophage-targeting ability, which is in agreement with the in vitro results (Figures 6H and 7).

Routine blood counts and coagulation indices, including TAT, D-dimer, and fibrinogen levels, were also evaluated. Compared with LPS-induced septic mice, both MPDA@SMI-4a@PEI/siPIM1 and MPDA@SMI-4a@PEI/siPIM1@GM treatments increased platelet counts in the blood, whereas the MPDA@SMI-4a@PEI/siPIM1@GM group showed a more obvious increase (**Figure** 9A). The plasma levels of TAT, D-dimer, and fibrinogen in the MPDA@SMI-4a@PEI/siPIM1- and MPDA@SMI-4a@PEI/siPIM1@GM-treated groups were lower than those in the LPS group. Notably, the MPDA@SMI-4a@PEI/siPIM1@GM-treated group demonstrated lower plasma TAT, D-dimer, and fibrinogen levels than the MPDA@SMI-4a@PEI/siPIM1 group (Figure 9B–D).

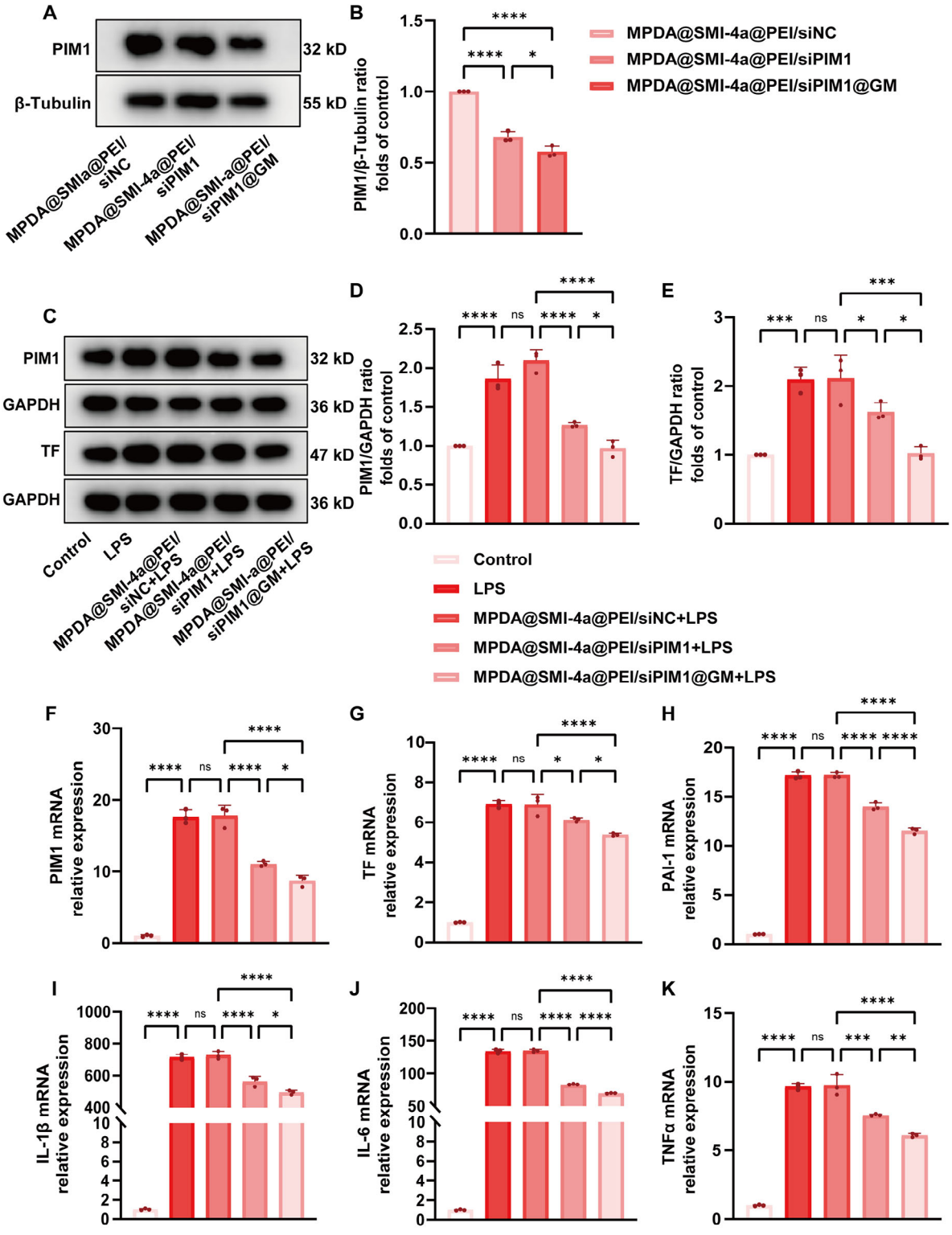

Figure 7. NPs knock down PIM1 expression and reduce the expression of TF in RAW264.7 cells. A) Western blot images and corresponding densitometric analyses of B) PIM1 expression in RAW264.7 pretreated with different NPs (n = 3). C) Western blot images and corresponding densitometric analyses of D) PIM1 and E) TF expression in RAW264.7 cells (n = 3). F–K) mRNA expression of F) PIM1, G) TF, H) PAI-1, I) IL-1β, J) IL-6, and K) TNF-α measured by RT-qPCR. Each bar represents the mean ± SD. Statistical analysis for three or more groups was carried out using one-way ANOVA (B and D–K). * $p < 0.05$, ** $p < 0.01$, *** $p < 0.001$, **** $p < 0.0001$.

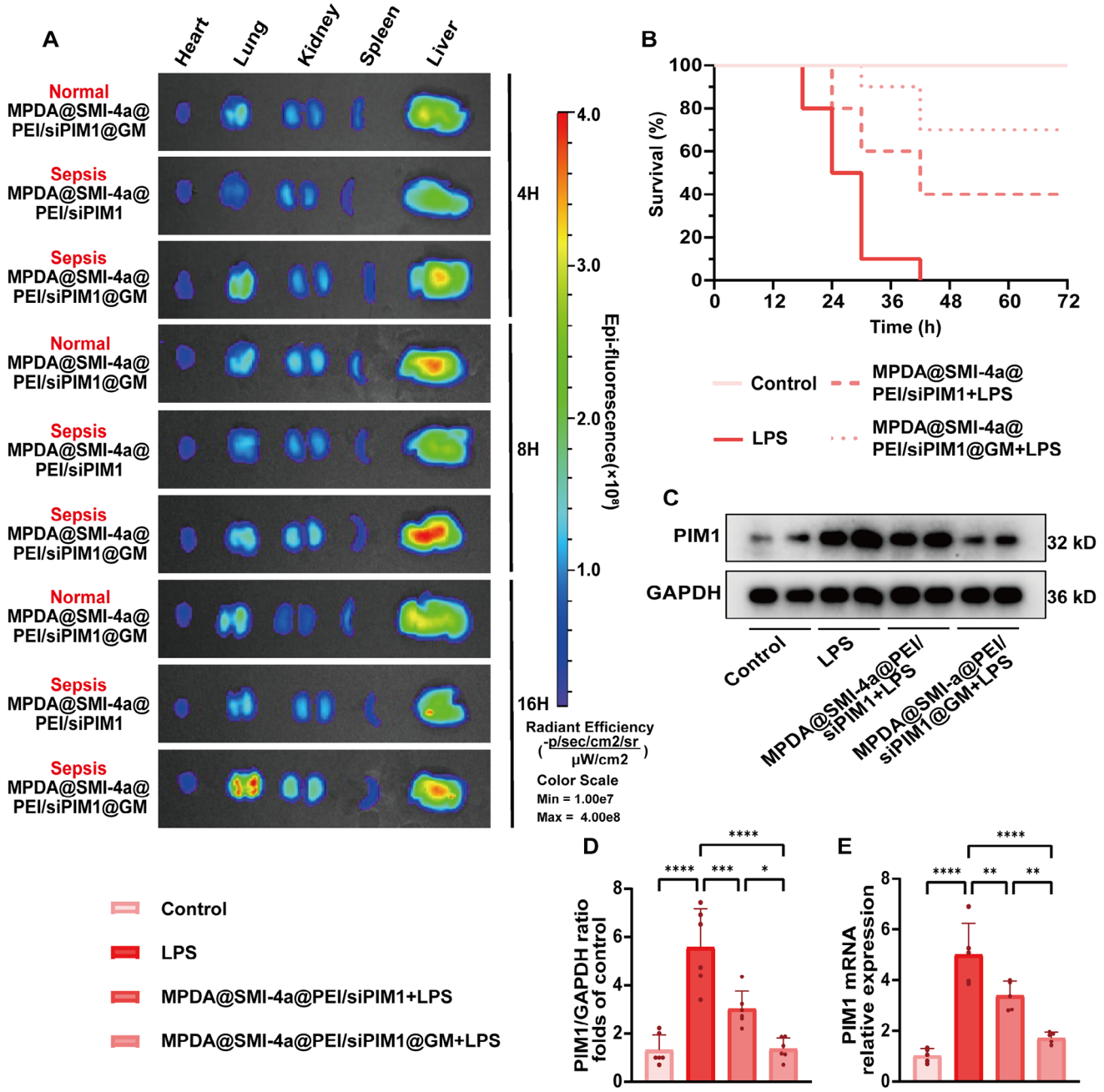

Figure 8. In vivo therapeutic effect of NPs in LPS-induced septic mouse model. A) Ex vivo NIR imaging of major organs (heart, lung, kidneys, spleen, and liver) in mice. B) Survival rate of septic mice within 72 h after different treatments (n = 10/group). C) Western blot images and corresponding densitometric analyses of (D) PIM1 expression in the lung tissue (n = 6/group). E) mRNA expression of PIM1 in lung tissue measured by RT-qPCR (n = 5). Each bar represents the mean ± SD. Statistical analysis for three or more groups was carried out using one-way ANOVA (D and E). * $p < 0.05$, ** $p < 0.01$, *** $p < 0.001$, **** $p < 0.0001$.

Consistently, the protein expression levels of TF, PAI-1, and thrombin in the lung tissues of septic mice were notably reduced after treatment with MPDA@SMI-4a@PEI/siPIM1 (Figure 9E–I). These results indicate that MPDA@SMI-4a@PEI/siPIM1@GM improved the hypercoagulable state in septic mice.

Correspondingly, inflammatory cytokine production in the MPDA@SMI-4a@PEI/siPIM1@GM-treated group was significantly reduced compared to that in the LPS group (Figure 9J–L). Furthermore, we performed HE and immunohistochemistry analyses of the lung tissues. In the MPDA@SMI-4a@PEI/siPIM1@GM-treated group, alveolar edema and thickening were significantly alleviated and the microthrombus was reduced compared to the LPS group, as observed in pathological sections of the lung. Fibrin deposition and macrophage infiltration in the lungs were also ameliorated

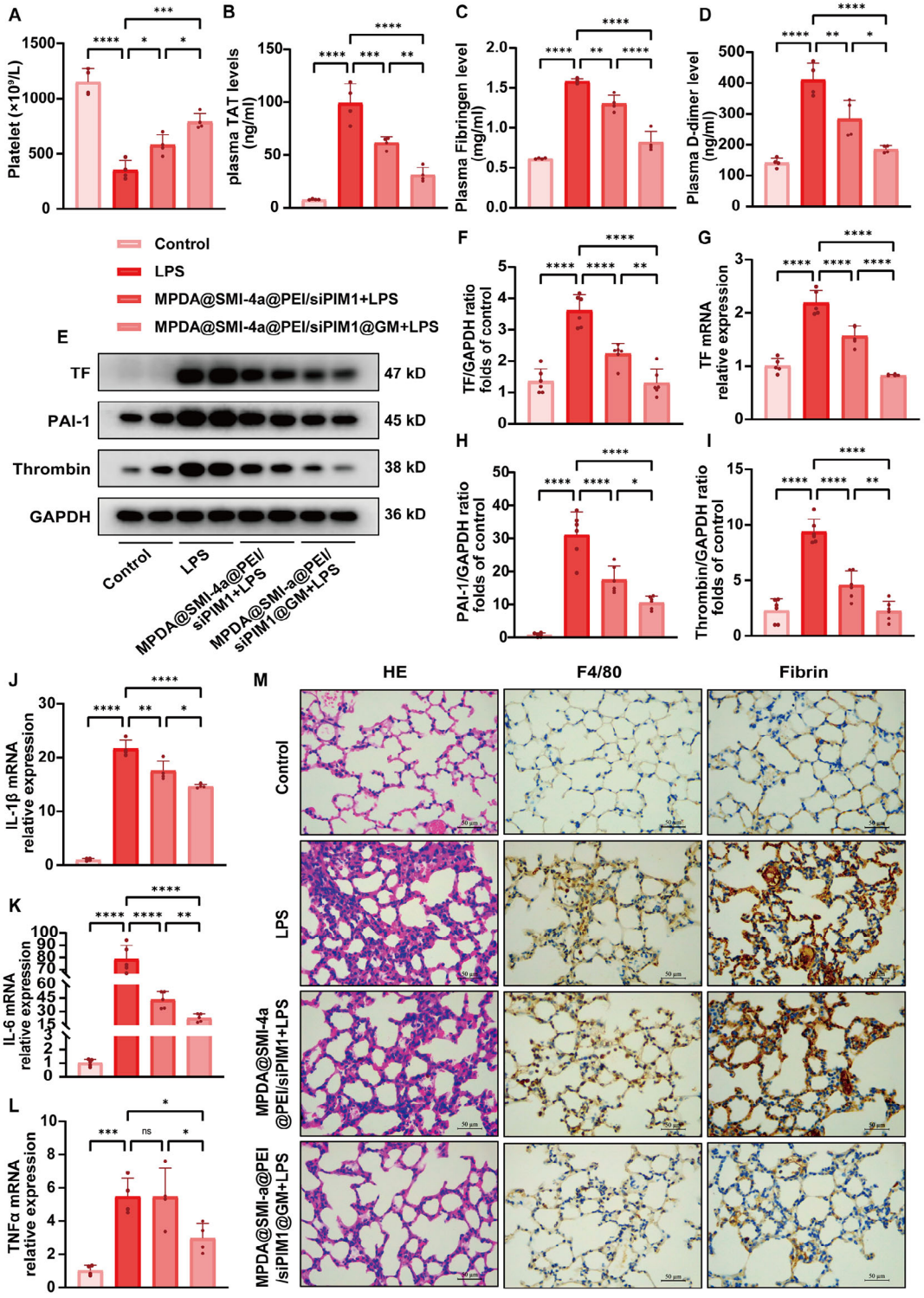

Figure 9. NPs protect septic mice against sepsis-induced coagulopathy and acute lung injury. A) Platelet count in mice (n = 4/group). B–D) Plasma levels of coagulation-related factors in mice plasma by ELISA, including (B) TAT, (C) fibrinogen, and (D) D-dimer (n = 4/group). E) Representative western blot membranes and corresponding densitometric analyses of (F) TF, (H) PAI-1, (I) Thrombin in lung tissue (n = 6/group). G) mRNA levels of TF in murine lung tissues (n = 5/group). J–L) mRNA levels of (J) IL-1β, (K) IL-6, and (L) TNF-α in murine lung tissues (n≥4/group). M) The lung sections were subjected to HE staining, F4/80 and fibrin immunohistochemical analysis (n = 4/group; scale bar: 50 μm). Each bar represents the mean ± SD. Statistical analysis for three or more groups was carried out using one-way ANOVA (A–D, F–I, and J–L). * $p < 0.05$, ** $p < 0.01$, *** $p < 0.001$, **** $p < 0.0001$.

in the NP-treated group (Figure 9M). These data suggest that MPDA@SMI-4a@PEI/siPIM1@GM possesses excellent targeting ability against sepsis-induced coagulation and ALI in vivo.

3. Conclusion

In this study, we identified PIM1 as a critical gene in patients with sepsis using RNA-seq and bioinformatic analyses combined with clinical research. Correlation analysis between PIM1 and coagulation factors revealed a significant positive association. In patients with sepsis, PIM1 exhibited great prognostic value for 28-day mortality and showed a strong correlation with traditional coagulation indices. In septic mice, upregulated PIM1 promoted the release of TF, resulting in activation of the coagulation cascade and ALI. Inhibiting the expression of PIM1 downregulated the phosphorylation of mTOR through the AKT and MAPK signaling pathways, leading to a reduction in TF release, correction of coagulation disorders, and alleviation of ALI. Inspired by these findings, a multifunctional MPDA@PEI@GM carrier with macrophage-targeting and ROS-scavenging abilities was developed to co-deliver the PIM1 inhibitors SMI-4a and siPIM1 to reduce PIM1 expression and improve SIC. Both in vitro and in vivo experiments demonstrated that MPDA@SMI-4a@PEI/siPIM1@GM effectively inhibited the expression of PIM1 in macrophages, normalized coagulation disorders, alleviated lung injury, and improved survival rates. Overall, the novel target PIM1 together with MPDA@SMI-4a@PEI/siPIM1@GM delivery systems may provide an applicable strategy for treating patients with SIC.

4. Experimental Section

Ethics Statement: The study was approved by the Ethics Committee of The First Affiliated Hospital of Wenzhou Medical University and complied with the principles of the Declaration of Helsinki (ethics approval number: KY2024-R212). Informed consent was obtained from all the participants or their next of kin. All the mouse experiments adhered to the Regulations for the Administration of Affairs Concerning Experimental Animals and the guidelines of the Animal Review Committee of The First Affiliated Hospital of Wenzhou Medical University (ethics approval number: WYYY-IACUC-AEC-2024-076).

Data Collection and Processing of RNA Transcriptome Sequencing: This work searched the GEO database (https://www.ncbi.nlm.nih.gov/gds/) with the keywords "sepsis"[MeSH Terms] AND "Homo sapiens"[porgn] AND "Expression profiling by array"[Filter] AND ("500"[n_samples]: "1000"[n_samples]) and obtained seven datasets. After excluding datasets for which samples were from pediatric sepsis or without complete clinical survival information, only the GSE65682 dataset met the inclusion criteria. In this dataset, there were 479 patients with sepsis with complete survival status data and 42 healthy controls. The "limma" package in R software (version 3.40.6) was used to analyze the differential expression. The DEGs were defined as those with a Student's *t*-test $p < 0.05$ and fold-change (FC) ≥ 1.5. To explore the DEG-related signal pathways and biological function, the "cluster profiler" and "GOplot" packages were applied to perform the KEGG and GO enrichment analyses. This work used the CIBERSORT algorithm to quantify the relative proportion of immune cell infiltration between patients with sepsis and healthy controls. In addition, 77 intersecting genes were obtained between the GSE65682 and RAW264.7 datasets using an online tool for analyses of Venn diagrams. Multivariate Cox regression and LASSO-Cox regression analyses were performed using the GSE65682 dataset to screen candidate genes and construct prediction models, respectively. Additionally, the risk score for each case in both prediction models was calculated. Based on the optimal cutoff value of the risk score, patients with sepsis were divided into low- and high-risk groups, and the survival time between the two groups was compared using Kaplan-Meier analysis. Moreover, we performed time-dependent ROC curve analysis to evaluate the discrimination ability of the risk score by using the "survival," "survivminer," and "timeROC" packages. Using a Venn diagram to compare the overlapping regions of the candidate genes screened using multivariate Cox regression and LASSO-Cox regression, we identified two overlapping genes. Furthermore, we performed a correlation analysis between coagulation factors (F2 and F3) and the two key genes screened below using the "ggstatsplot" and "ggplot2" packages to illustrate the results.

RNA Transcriptome Sequencing: RAW264.7 cells were seeded at equal densities into 6-well cell culture plates for 24 h. Three experimental groups were set up: a control group receiving growth medium alone, a group treated with 1 μg mL^{-1} LPS for 6 h, and a PIM1 inhibitor SMI-4a treatment group. The SMI-4a treatment group was pretreated with 80 μmol (final concentration) SMI-4a for 1 h before being treated with 1 μg mL^{-1} LPS for 6 h. After 6 h, the supernatant was aspirated and the cells were gently rinsed twice with 1 mL of PBS. A total of 960 μL RZ was added per well and was collected into RNase-free tubes, and stored at −80 °C. The samples were sent to LC Biotech (Hangzhou, China) on dry ice for RNA extraction and library construction. Bioinformatic analysis and visualization of the results were performed using OmicStudio (https://www.omicstudio.cn/tool).

Human Subjects: Patients diagnosed with sepsis in the intensive care unit (ICU) of The First Affiliated Hospital of Wenzhou Medical University from August 2023 and November 2023 who participated in the digital PCR study were enrolled in this study. The diagnostic criteria for sepsis were based on the Sepsis 3.0. According to the International Society on Thrombosis and Hemostasis diagnostic criteria for DIC and SIC, the enrolled patients were divided into DIC and non-DIC groups, and SIC and non-SIC groups. Based on the survival status, the enrolled patients with sepsis were separated into two groups: survivors and non-survivors.

Data Collection and Blood Sample Measurements: Demographic data were collected for each patient. Clinical data, including the source of infection, platelet counts, PT, APTT, INR, fibrinogen, and lactate concentrations, were obtained and recorded within the first 24 h of admission. 5 mL of peripheral venous blood were collected within 24 h after ICU admission, then plasma was isolated and frozen at −80 °C for subsequent experiments.

Animals: C57BL/6J mice (male, 8 weeks old) were obtained from Beijing Vital River Laboratory Animal Technology, China. All animals were housed in the laboratory animal center of The First Affiliated Hospital of Wenzhou Medical University and maintained under specific pathogen-free conditions.

LPS-Induced Septic Mouse Model: To establish a sepsis mouse model, mice were administered intraperitoneally with 0.4 mg kg^{-1} of LPS (Sigma-Aldrich, L2630). After 7 h, a 12-h stimulation was induced by another intraperitoneal injection of 10 mg kg^{-1} LPS.[35,36] In the SMI-4a treatment group, 20 mg kg^{-1} of SMI-4a was administered 1 h before LPS stimulation. In the NP-treated group, NPs (siRNA 0.28 mg kg^{-1})[37] were administered following LPS stimulation. The lung tissues were removed and fixed in 4% paraformaldehyde or immediately stored at −80 °C. The whole blood was centrifuged at 1000 × g for 15 min, and the plasma was collected and stored at −80 °C.

Histopathological Analysis and Immunohistochemistry: All mice were sacrificed, and the separated lung tissues were fixed, dehydrated, embedded, sectioned, and deparaffinized. Next, the sections were stained with HE for histological examination. For immunohistochemical staining, the slices were steamed in a citric acid buffer to expose the antigen-binding sites. After blocking with 1% bovine serum albumin (BSA, BD Biosciences), primary antibodies against PIM1 (1:50, #48896, SAB), F4/80 (1:100, Servicebio, Wuhan, China) and fibrin (1:100, Servicebio, Wuhan, China) were added and incubated overnight at 4 °C. After using HRP-conjugated goat anti-rabbit secondary antibody, diaminobenzidine staining, and counterstaining with hematoxylin, the expression of PIM1, F4/80, and fibrinogen was imaged under light microscopy.

Enzyme-Linked Immunosorbent Assay: The concentrations of PIM1 (CSB-E11825 h, Cusabio, China) in human plasma and TAT (CSB-E08433 m, Cusabio, China), Fbg (CSB-E08202 m, Cusabio, China), and D2D (CSB-E13584 m, Cusabio, China) in mouse plasma were assessed using ELISA kits according to the guidelines outlined in the respective ELISA kits.

Cell Culture and Treatments: DMEM with 10% FBS was used to culture RAW264.7 cells (ATCC, USA) at 37 °C with 5% CO_2. RAW264.7 cells were seeded into 6-well or 12-well plates overnight until 60%–70% confluence was reached. Then, RAW264.7 cells were treated with or without SMI-4a for 1 h before being stimulated with LPS (1 μg mL^{-1}) for 6 h.

Cell Viability: A Cell-Counting Kit 8 (HY-K0301, MCE, USA) was used to evaluate the relative cell viability. RAW264.7 cells were seeded in 96-well plates (1×10^4 cells $well^{-1}$) and incubated overnight. The cells were then incubated with the corresponding treatment, and the culture supernatant was replaced with fresh 10% CCK-8 medium at the indicated times. Finally, absorbance was measured at 450 nm using a multimode microplate reader.

Western Blotting: Protein samples were extracted from the lung tissue and RAW264.7 cells with RIPA buffer (539134, Millipore, MA, USA) supplemented with protease and phosphatase inhibitor tablets (524628, Millipore), and then quantified using the BCA kit. Protein electrophoresis was performed on a 10% SDS-PAGE gel and the proteins were transferred onto a nitrocellulose membrane (IPVH85R, Millipore). The membranes were blocked in 5% skim milk before being incubated overnight at 4 °C with the following primary antibody: anti-PIM1 (#48896, SAB), anti-TF (DF6400, Affinity), anti-thrombin (ab314480, Abcam), anti-PAI-1 (ab22275, Abcam), anti-p-mTOR (5536T, CST), anti-mTOR (2983T, CST), anti-p-p70s6k (9234T, CST), anti-p70s6k (34475T, CST), anti-p-ERK1/2 (4370T, CST), anti-ERK1/2 (4695T, CST), anti-p-AKT (4060T, CST), and anti-AKT (4691T, CST). The membranes were washed and incubated with a secondary antibody for 1 h at ≈20 –25 °C. Protein signals were detected using enhanced chemiluminescence reagents and quantified using ImageJ software.

Immunofluorescence Staining: RAW264.7 cells were seeded in 12-well plates with the corresponding treatment. Then the cells were fixed, permeabilized, blocked, and incubated overnight at 4 °C with primary antibodies. Subsequently, a fluorescent secondary antibody was used in the dark at 37 °C for 1 h. Finally, sections were counterstained with an anti-fluorescence quencher containing DAPI. A fluorescence microscope was used to capture the images.

RNA Extraction and Quantitative Real-Time PCR Analysis: Total RNA was extracted from lung tissue or cells using the RNA Simple Total RNA Kit (Tiangen, China). Next, the purified RNA (1000 ng) was reverse-transcribed into cDNA using the All-In-One 5 × RT MasterMix. SYBR Green (Roche Diagnostics, Germany) and CFX Opus 96 (Bio-Rad, USA) were used to analyze the mRNA expression. Finally, gene expression was normalized to that of GAPDH. The primer sequences are listed in Table S1, Supporting Information.

siRNA Transfection: Control siRNA (siNC) and PIM1 siRNA (siPIM1) were synthesized by GenePharma (China). The sequence of siNC is as follows: S: 5′-UUCUCCGAACGUGUCACGUTT-3′; AS: 5′-ACGUGACACGUUCGGAGAATT-3. ' The sequence of siPIM1 is as follows: S: 5′-UGCAAGACCUCUUCGACUUUATT-3′; AS: 5′-UAAAGUCGAAGAGGUCUUGCATT-3. ' Transient transfection of siRNA into RAW264.7 cells was performed with siRNA using the Lipofectamine RNAiMAX Reagent. RAW264.7 cells were transfected with 100 nM siRNA and cultured for 48 h, then subsequent experiments were performed.

Synthesis of Nanomaterials: SMI-4a powder (10 mg) was dissolved in an aqueous solution containing 1 mL of absolute ethanol (10 mg mL^{-1}). Next, 100 μL SMI-4a aqueous solution and 200 μL MPDA aqueous dispersion (10 mg mL^{-1}) were added to 1.8 mL absolute ethanol and stirred at room temperature for 24 h. Next, 16 mg of PEI (molecular weight of 1800 kD) dissolved in 500 μL deionized water was added to the mixture and stirred for the next 24 h. Subsequently, the mixture was centrifuged at 3720 × g for 5 min and washed three times with deionized water. Finally, the mixture was lyophilized and resuspended in nuclease-free water for future use.

Characterization of MPDA@SMI-4a@PEI NPs: The size distribution and surface charge density of the nanomaterials were determined using an NP-tracking analysis instrument (Particle Metrix GmbH, Germany). The morphology of the MPDA@SMI-4a@PEI NPs was examined using field-emission transmission electron microscopy (TEM; JEM-F200, JEOL, Japan).

Nanomaterials Targeting Ability: Immunofluorescence: RAW264.7 cells were seeded into a 15 mm confocal culture dish (1×10^5 cells $dish^{-1}$) for 24 h. Next, the siRNA was incubated with YOYO-1 green fluorescent dye for 2 h. Different nanoparticles were then used to transfect siRNA dyed with YOYO-1 into RAW264.7 cells. After washing three times with PBS for 4 h, the cells were fixed with 1 mL of 4% paraformaldehyde for 10 min and treated with 1 mL of 0.5% Triton-X-100 for 5 min. Then, 200 μL of red fluorescent phalloidin staining reagent (BL1189A, Biosharp) was added and incubated at 37 °C for 30 min. Then, the cells were washed three times with PBS and mixed with 200 μL DAPI (C0065, Solarbio) for 1 min. Finally, images were obtained using a laser confocal microscope (Stellaris 5, Leica, Germany).

Nanomaterials Targeting Ability: Flow Cytometry: RAW264.7 cells were seeded into 6-well plates (1×10^5 cells $well^{-1}$) for 24 h. After the same treatment described above, the cells were harvested and analyzed within 1 h using CytoFLEX (Beckman Coulter Biotechnology, China).

ROS-Scavenging Capacity: The Reactive Oxygen Species Assay Kit (S0033S, Beyotime) was used to determine ROS levels. RAW264.7 cells were seeded in 6-well plates (1×10^5 cells $well^{-1}$) for 24 h. The MPDA@SMI-4a@PEI NPs were added to the wells with and without LPS stimulated for 24 h. Then the culture supernatant was replaced with 10 μmol L^{-1} DCFH-DA fresh medium without serum and incubated at 37 °C for 20 min. Finally, the cells were harvested and analyzed using CytoFLEX (Beckman Coulter Biotechnology).

In Vivo Biodistribution: MPDA@SMI-4a@PEI/siPIM1 or MPDA@SMI-4a@PEI/siPIM1@GM NPs were prepared, where MPDA@SMI-4a @PEI was pre-labeled with a Sulfo-Cyanine5.5 NHS ester tripotassium fluorescent probe (HY-D1389, MCE, China). The mice were divided into three groups: 1) healthy mice + MPDA@SMI-4a@PEI/siRNA@GM, 2) LPS-induced septic mice + MPDA@SMI-4a@PEI/siRNA, and 3) LPS-induced septic mice + MPDA@SMI-4a@PEI/siRNA@GM. Mice were sacrificed at 4, 8, and 16 h after NPs administration. Major organs were collected for ex vivo imaging using an in vitro imaging system (IVIS Lumina Series III; PerkinElmer, USA).

Statistical Analysis: Statistical calculations were performed using GraphPad Prism version 9.0.0. Statistical significance for binary comparisons was assessed using Student's *t*-test. For a comparison of more than two groups, one-way ANOVA was used. Statistical significance was set at $p < 0.05$. In the clinical cohort, SPSS Version 26 was used for the statistical analyses. Diagnostic accuracy was determined by calculating the AUC with a 95% confidence interval. Unless otherwise indicated, data are represented as the means ± SD.

Supporting Information

Supporting Information is available from the Wiley Online Library or from the author.

Acknowledgements

This work was supported by the National Natural Science Foundation of China (82272204, 82472188, 52203336), "Pioneer" and "Leading Goose" R&D Program of Zhejiang (2023C03084) and the project of Wenzhou major science and technology innovation (ZY2023005).

Conflict of Interest

The authors declare no conflict of interest.

Data Availability Statement

Data supporting the findings of this study are available from the corresponding author upon request.

Keywords

coagulation in sepsis, co-delivery, multifunctional carriers, PIM1, transcriptomics

Received: December 27, 2024
Revised: March 12, 2025
Published online: March 26, 2025

[1] M. Singer, C. S. Deutschman, C. W. Seymour, M. Shankar-Hari, D. Annane, M. Bauer, R. Bellomo, G. R. Bernard, J.-D. Chiche, C. M. Coopersmith, R. S. Hotchkiss, M. M. Levy, J. C. Marshall, G. S. Martin, S. M. Opal, G. D. Rubenfeld, T. van der Poll, J.-L. Vincent, D. C. Angus, *JAMA, J. Am. Med. Assoc.* **2016**, *315*, 801.
[2] V. Liu, G. J. Escobar, J. D. Greene, J. Soule, A. Whippy, D. C. Angus, T. J. Iwashyna, *JAMA, J. Am. Med. Assoc.* **2014**, *312*, 90.
[3] K. E. Rudd, S. C. Johnson, K. M. Agesa, K. A. Shackelford, D. Tsoi, D. R. Kievlan, D. V. Colombara, K. S. Ikuta, N. Kissoon, S. Finfer, C. Fleischmann-Struzek, F. R. Machado, K. K. Reinhart, K. Rowan, C. W. Seymour, R. S. Watson, T. E. West, F. Marinho, S. I. Hay, R. Lozano, A. D. Lopez, D. C. Angus, C. J. L. Murray, M. Naghavi, *Lancet* **2020**, *395*, 200.
[4] S. Gando, M. Levi, C.-H. Toh, *Nat. Rev. Dis. Primers* **2016**, *2*, 16037.
[5] M. Levi, M. Scully, *Blood* **2018**, *131*, 845.
[6] M. Di Nisio, F. Baudo, B. Cosmi, A. D'Angelo, A. De Gasperi, A. Malato, M. Schiavoni, A. Squizzato, *Thromb. Res.* **2012**, *129*, 177.
[7] J.-L. Vincent, B. Francois, I. Zabolotskikh, M. K. Daga, J.-B. Lascarrou, M. Y. Kirov, V. Pettilä, X. Wittebole, F. Meziani, E. Mercier, S. M. Lobo, P. S. Barie, M. Crowther, C. T. Esmon, J. Fareed, S. Gando, K. J. Gorelick, M. Levi, J.-P. Mira, S. M. Opal, J. Parrillo, J. A. Russell, H. Saito, K. Tsuruta, T. Sakai, D. Fineberg, for the S. T. Group, *JAMA, J. Am. Med. Assoc.* **2019**, *321*, 1993.
[8] E. Abraham, K. Reinhart, S. Opal, I. Demeyer, C. Doig, A. L. Rodriguez, R. Beale, P. Svoboda, P. F. Laterre, S. Simon, B. Light, H. Spapen, J. Stone, A. Seibert, C. Peckelsen, C. De Deyne, R. Postier, V. Pettilä, C. L. Sprung, A. Artigas, S. R. Percell, V. Shu, C. Zwingelstein, J. Tobias, L. Poole, J. C. Stolzenbach, A. A. Creasey, *JAMA, J. Am. Med. Assoc.* **2003**, *290*, 238.
[9] B. L. Warren, A. Eid, P. Singer, S. S. Pillay, P. Carl, I. Novak, P. Chalupa, A. Atherstone, I. Pénzes, A. Kübler, S. Knaub, H.-O. Keinecke, H. Heinrichs, F. Schindel, M. Juers, R. C. Bone, S. M. Opal, for the K. T. S. Group, *JAMA, J. Am. Med. Assoc.* **2001**, *286*, 1869.
[10] J. L. Vincent, M. K. Ramesh, D. Ernest, S. P. LaRosa, J. Pachl, N. Aikawa, E. Hoste, H. Levy, J. Hirman, M. Levi, M. Daga, D. J. Kutsogiannis, M. Crowther, G. R. Bernard, J. Devriendt, J. V. Puigserver, D. U. Blanzaco, C. T. Esmon, J. E. Parrillo, L. Guzzi, S. J. Henderson, C. Pothirat, P. Mehta, J. Fareed, D. Talwar, K. Tsuruta, K. J. Gorelick, Y. Osawa, I. Kaul, *Crit. Care Med.* **2013**, *41*, 2069.
[11] H. Saito, I. Maruyama, S. Shimazaki, Y. Yamamoto, N. Aikawa, R. Ohno, A. Hirayama, T. Matsuda, H. Asakura, M. Nakashima, N. Aoki, *J. Thromb. Haemost.* **2006**, *5*, 31.
[12] T. Iba, D. Saito, H. Wada, H. Asakura, *Thromb. Res.* **2012**, *130*, 129.
[13] S. P. Grover, N. Mackman, *ATVB* **2018**, *38*, 709.
[14] T. van der Poll, F. L. van de Veerdonk, B. P. Scicluna, M. G. Netea, *Nat. Rev. Immunol.* **2017**, *17*, 407.
[15] R. Pawlinski, J.-G. Wang, A. P. Owens, J. Williams, S. Antoniak, M. Tencati, T. Luther, J. W. Rowley, E. N. Low, A. S. Weyrich, N. Mackman, *Blood* **2010**, *116*, 806.
[16] E. M. Egorina, M. A. Sovershaev, J. O. Olsen, B. Østerud, *Blood* **2008**, *111*, 1208.
[17] R. Pawlinski, B. Pedersen, G. Schabbauer, M. Tencati, T. Holscher, W. Boisvert, P. Andrade-Gordon, R. D. Frank, N. Mackman, *Blood* **2004**, *103*, 1342.
[18] L. Tan, Y. Huang, X. Pan, S. Quan, S. Xu, D. Li, L. Song, X. Zhang, W. Chen, J. Pan, *Ann. Medicine* **2016**, *48*, 235.
[19] S. Xu, Z. Zhou, H. Li, Z. Liu, X. Pan, F. Wang, Y. Huang, X. Li, Y. Xiao, J. Pan, C. Wang, D. Li, *J. Cell Sci.* **2017**, *131*, 211151.
[20] Y. Sun, F. Ye, D. Li, H. Yang, T. Xu, X. Zhong, Y. Lu, H. Zhou, J. Pan, *Toxicol. Appl. Pharmacol* **2023**, *460*, 116364.
[21] Y. Lu, D. Li, Y. Huang, Y. Sun, H. Zhou, F. Ye, H. Yang, T. Xu, S. Quan, J. Pan, *JIR* **2023**, *16*, 1027.
[22] J. Bi, Y. Wang, K. Wang, Y. Sun, F. Ye, X. Wang, J. Pan, *Biochimica et Biophysica Acta (BBA)* **2024**, *1870*, 167281.
[23] X. F. Hu, J. Li, S. Vandervalk, Z. Wang, N. S. Magnuson, P. X. Xing, *J. Clin. Invest.* **2009**, *119*, 362.
[24] R. Fu, Y. Xia, M. Li, R. Mao, C. Guo, M. Zhou, H. Tan, M. Liu, S. Wang, N. Yang, J. Zhao, *Arthritis Rheumatol.* **2019**, *71*, 1308.
[25] M. Bellon, L. Lu, C. Nicot, *Blood* **2016**, *127*, 2439.
[26] Y. S. Shin, K. Takeda, Y. Shiraishi, Y. Jia, M. Wang, L. Jackson, A. D. Wright, L. Carter, J. Robinson, E. Hicken, E. W. Gelfand, *Am. J. Respir. Cell Mol. Biol.* **2012**, *46*, 488.
[27] S. Xu, X. Pan, L. Mao, H. Pan, W. Xu, Y. Hu, X. Yu, Z. Chen, S. Qian, Y. Ye, Y. Huang, J. Pan, *Cell Commun. Signal* **2020**, *18*,104.
[28] X. Dai, Z. Liu, X. Zhao, K. Guo, X. Ding, F. Xu, N. Zhao, *Adv. Mater.* **2024**, *36*, 2407927.
[29] Y. Wei, X. Li, J. Lin, Y. Zhou, J. Yang, M. Hou, F. Wu, J. Yan, C. Ge, D. Hu, L. Yin, *Adv. Mater.* **2023**, *35*, 22068.
[30] M. Fernández-Delgado, M. S. Sirsat, E. Cernadas, S. Alawadi, S. Barro, M. Febrero-Bande, *Neural. Netw* **2019**, *111*, 11.
[31] W. L. Cheung-Lee, A. J. Link, *J. Ind. Microbiol. Biotechnol.* **2019**, *46*, 1371.
[32] K. Søreide, *J. Clin. Pathol.* **2009**, *62*, 1.
[33] B. Williams, L. Zou, J.-F. Pittet, W. Chao, *Anesthesia Analg* **2024**, *138*, 696.
[34] A. Amaral, S. M. Opal, J.-L. Vincent, *Intensive Care Med.* **2004**, *30*, 1032.
[35] L. Ba, J. Gao, Y. Chen, H. Qi, C. Dong, H. Pan, Q. Zhang, P. Shi, C. Song, X. Guan, Y. Cao, H. Sun, *Phytomedicine* **2019**, *58*, 152765.
[36] J. A. Hagar, D. A. Powell, Y. Aachoui, R. K. Ernst, E. A. Miao, *Science* **2013**, *341*, 1250.
[37] T. Jeon, D. C. Luther, R. Goswami, C. Bell, H. Nagaraj, Y. A. Cicek, R. Huang, J. A. Mas-Rosario, J. L. Elia, J. Im, Y.-W. Lee, Y. Liu, F. Scaletti, M. E. Farkas, J. Mager, V. M. Rotello, *ACS Nano* **2023**, *17*, 4315.

